Title

Experimental partitioning of Ca isotopes and Sr into anhydrite: Consequences for the cycling of Ca and Sr in subseafloor mid-ocean ridge hydrothermal systems

Authors

Syverson, Drew D
Scheuermann, Peter
Higgins, John A
et al.

Publication Date

2018-09-01

DOI

10.1016/j.gca.2018.03.018

Peer reviewed

Available online at www.sciencedirect.com

ScienceDirect

Geochimica et Cosmochimica Acta xxx (2018) xxx–xxx

Geochimica et Cosmochimica Acta

www.elsevier.com/locate/gca

Experimental partitioning of Ca isotopes and Sr into anhydrite: Consequences for the cycling of Ca and Sr in subseafloor mid-ocean ridge hydrothermal systems

Drew D. Syverson [a,b,c,*], Peter Scheuermann [b], John A. Higgins [d], Nicholas J. Pester [e], William E. Seyfried Jr. [b]

[a] Yale University, Department of Geology and Geophysics, 210 Whitney Ave., New Haven, CT 06511, USA
[b] University of Minnesota, Department of Earth Sciences, 310 Pillsbury Drive SE, Minneapolis, MN 55455-0231, USA
[c] Monash University, Department of Earth, Atmosphere and Environment, 9 Rainforest Walk, Building 28, Clayton, VIC 3800, Australia
[d] Princeton University, Department of Geosciences, Guyot Hall, Princeton, NJ 08544, USA
[e] Lawrence Berkeley National Laboratory, One Cyclotron Road, Berkeley, CA 94720, USA

Received 2 August 2017; accepted in revised form 20 March 2018; available online xxxx

Abstract

The elemental and isotopic mass balance of Ca and Sr between seawater and the oceanic crust at mid-ocean ridge (MOR) hydrothermal systems integrates various physiochemical processes in the subseafloor, such as dissolution of primary silicate minerals, formation of secondary minerals, and phase separation in the subseafloor. In particular, the precipitation and recrystallization of anhydrite are recognized as important processes controlling the Ca and Sr elemental and isotope composition of high temperature vent fluids and coexisting ocean crust, and yet, little experimental data exist to constrain the mechanism and magnitude of these critical geochemical effects. Thus, this study experimentally examines Sr/Ca partitioning, Ca isotope fractionation, and the rate of exchange between anhydrite and dissolved constituents. These experimental constraints are then compared with Sr/Ca and Ca isotope compositions of anhydrite and vent fluids sampled from the TAG hydrothermal system. Accordingly, anhydrite precipitation and recrystallization experiments were performed at 175, 250, and 350 °C and 500 bar at chemical conditions characteristic of active MOR hydrothermal systems. Experimental data suggest that upon entrainment and recharge of seawater into MOR hydrothermal systems anhydrite will rapidly precipitate with a Ca isotopic composition that is depleted in the heavy isotope compared to the hydrothermal fluid. The magnitude of the Ca isotope fractionation, $\Delta^{44/40}Ca_{(Anh\text{-}Fluid)}$, is temperature dependent, −0.45, −0.22, and −0.02‰, for 175, 250, and 350 °C, respectively, but likely indicative of kinetic effects. Utilization of a ^{43}Ca spike in solution was implemented to quantify the time-dependent extent of isotope exchange during anhydrite recrystallization at chemical equilibrium. These data indicate that the rate of exchange is a function of temperature, where 12, 46, and 45% exchange occurred within 1322, 867, 366 h at 175, 250, and 350 °C, respectively. The partitioning of Sr/Ca between anhydrite and constituent dissolved species during precipitation depends greatly on the saturation state of the hydrothermal fluid with respect to anhydrite at each experimental temperature, $K_{D(Anh\text{-}Fluid)} = 1.24–0.55$ at 175–350 °C, broadly similar to results of earlier experimental observations by Shikazono and Holland (1983). Equilibrium $K_{D(Anh\text{-}Fluid)}$ values were estimated by taking explicit account of time dependent magnitude of exchange, yielding values of 0.43, 0.36, 0.29 at 175, 250, and 350 °C, respectively. Coupling these experimental constraints with the temperature gradient inferred for high temperature MOR hydrothermal systems suggests that the Ca isotope and Sr elemental composition of anhydrite formed near the seafloor will retain the composition derived upon initial formation conditions, which is indicative of disequilibrium. In contrast, at greater depths and at higher temperatures, anhydrite will reflect

* Corresponding author at: Yale University, Department of Geology and Geophysics, 210 Whitney Ave., New Haven, CT 06511, USA.
E-mail address: drew.syverson@yale.edu (D.D. Syverson).

https://doi.org/10.1016/j.gca.2018.03.018

Please cite this article in press as: Syverson D. D., et al. Experimental partitioning of Ca isotopes and Sr into anhydrite: Consequences for the cycling of Ca and Sr in subseafloor mid-ocean ridge hydrothermal systems. *Geochim. Cosmochim. Acta* (2018), https://doi.org/10.1016/j.gca.2018.03.018

close to equilibrium Sr/Ca partitioning and Ca isotope fractionation conditions. The experimental and natural data presented in this study can be used to further understand the effect of anhydrite precipitation during hydrothermal circulation in the oceanic crust and on the chemical and isotopic composition of seawater on geologic timescales.

Keywords: Anhydrite; Ca isotopes; Sr/Ca partitioning; Mid-ocean ridge hydrothermal systems

1. INTRODUCTION

The formation of anhydrite ($CaSO_4$) in active high temperature mid-ocean ridge (MOR) hydrothermal systems occurs as a consequence of conductive heating of Ca^{2+} and SO_4^{2-}-bearing seawater that is recharged into the oceanic crust and during mixing of high temperature hydrothermal fluid with seawater at vent sites on the seafloor (Fig. 1). This reaction is thought to be widespread in modern oceanic mid-ocean ridge hydrothermal systems due to the inherent retrograde solubility of anhydrite at pressure, temperature, and chemical conditions indicative of MOR hydrothermal systems and the high Ca^{2+} and SO_4^{2-} contents of modern seawater (Bischoff and Seyfried, 1978; Seyfried and Ding, 1993; Newton and Manning, 2004). However, in spite of the ubiquitous occurrence of anhydrite in high temperature MOR hydrothermal systems, very little anhydrite is preserved in older oceanic crust and the importance of subseafloor anhydrite as a long-term sink of seawater SO_4^{2-} and/or Ca^{2+} is controversial (Sleep, 1991; Alt, 1995; Teagle et al., 1998b; Alt et al., 2003). In addition to MOR hydrothermal systems, anhydrite also persistently forms in oceanic back-arc basin hydrothermal systems and in continental hosted porphyry hydrothermal deposits as a consequence of heating and mixing of fluids that are concentrated in Ca^{2+} and SO_4^{2-}. Geologic environment notwithstanding, anhydrite formation has important geophysical and geochemical implications for fluid flow in the crust, elemental cycling between rock and fluid reservoirs, and hydrothermal processes such as redox buffering and mineral deposition associated with the formation of economic ore deposits (Lowell et al., 2003; Ono et al., 2007; Tolstoy et al., 2008; Craddock et al., 2010; Peters et al., 2010; Blundy et al., 2015; McDermott et al., 2015; Nadeau, 2015).

Geochemical tracers that have been applied to the study of anhydrite formation in subseafloor hydrothermal systems include Sr content and $^{87}Sr/^{86}Sr$ ratios, $^{18}O/^{16}O$ ratios, and multiple S isotope ratios ($^{34}S/^{32}S$ and $^{33}S/^{32}S$) (Chiba et al., 1998; Teagle et al., 1998a; Mills and Tivey, 1999; Ono et al., 2007; Peters et al., 2010). These applications benefit from experimental studies bearing on the redox and temperature dependent stability of anhydrite at elevated temperature and pressures (Ohmoto and Rye, 1979; Chiba et al., 1981; Ohmoto and Lasaga, 1982). In combination, these data have shown that seawater pervasively enters the subseafloor and mixes with high temperature hydrothermal fluids, inducing the formation of extensive sulfide deposits at and below the seafloor. In addition, these data have helped to constrain the degree of water-rock interaction in the subseafloor, while further documenting microbial effects that influence mass transfer of elements between seawater and the oceanic crust. However, complementary elemental and isotopic systems, such as Ca, have not been studied extensively and may provide important additional information that can further elucidate the temporal and spatial evolution of marine hydrothermal systems.

Previous experimental efforts precipitated anhydrite upon heating Ca and SO_4 bearing fluid, although equilibrium phase relations were not determined unambiguously (Shikazono and Holland, 1983). The experimental data reported here not only address anhydrite solubility, but also quantify the magnitude and sign of fractionation of Ca isotopes during anhydrite precipitation. These data benefit from careful analysis of the effect of temperature and time on the rate of exchange of Ca isotopes between anhydrite and dissolved Ca^{2+} species, with implications for interpretation of the physiochemical characteristics of active MOR and oceanic/continental volcanic arc hydrothermal systems, especially since anhydrite precipitation has been invoked as an important process in the Ca isotope budget of subseafloor hydrothermal systems but comparable experimental data are lacking (Amini et al., 2008).

With the continued advancement of multi-collector ICP-MS (MC-ICP-MS) technology and increasingly more sophisticated techniques and procedures for isotopic analysis and experimentation, the Ca isotope composition of hydrothermal fluids and coexisting minerals from MOR systems are now being determined to better understand subseafloor hydrothermal processes. However, there are few experimental data with respect to the Ca isotope system to broaden the interpretation of fluid and mineral alteration processes in natural hydrothermal systems. Furthermore, Ca isotopes can be used to trace rates and mechanisms of mass transfer in experimental studies, with important implications for testing equilibrium Sr/Ca partitioning, K_D, between anhydrite and fluid, despite incomplete exchange between distinct chemical reservoirs.

This study examines two important geochemical tracers, Ca isotope fractionation and partitioning of elemental Sr, during precipitation and recrystallization of anhydrite at 175, 250, and 350 °C and 500 bars at controlled chemical conditions in hydrothermal experiments. Experimental constraints are then compared with Ca and Sr elemental and isotopic compositions of hydrothermal fluid – anhydrite pairs recovered from the MOR hydrothermal systems, Logatchev and TAG, as presented by Amini et al. (2008) and this study, respectively. In addition, the experimental and natural data presented in this study are also compared with a limited number of measured end-member hydrothermal fluids from a variety of MOR hydrothermal systems

Please cite this article in press as: Syverson D. D., et al. Experimental partitioning of Ca isotopes and Sr into anhydrite: Consequences for the cycling of Ca and Sr in subseafloor mid-ocean ridge hydrothermal systems. *Geochim. Cosmochim. Acta* (2018), https://doi.org/10.1016/j.gca.2018.03.018

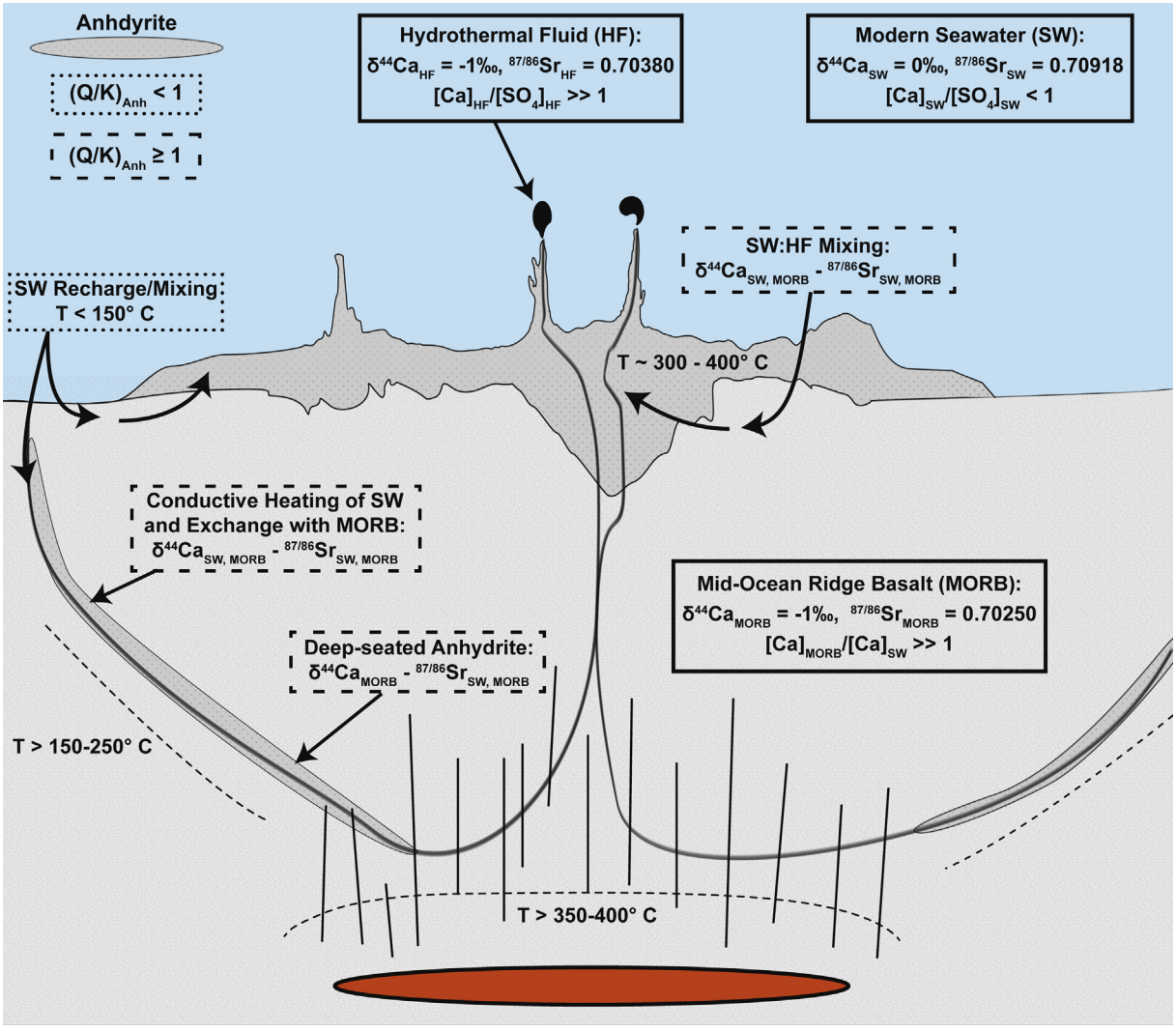

Fig. 1. Schematic diagram of the different zones of anhydrite at and below the seafloor, as indicated by the grey speckle areas. Dissolution of anhydrite, $(Q/K)_{Anh}$ <1 (dotted rectangle), occurs at low temperature, <150 °C, as a result of pervasive seawater mixing and subsequent cooling of the hydrothermal mound at and below the seafloor. Anhydrite precipitation, $(Q/K)_{Anh} \geq 1$ (dashed rectangles), occurs at temperatures > 150 °C and is a result of conductive heating of seawater and/or mixing with high temperature hydrothermal fluid. The chemical and isotopic composition of the sources of Ca, Sr, and SO_4 recorded by anhydrite upon formation are described by the solid rectangles. Each zone of anhydrite precipitation corresponds to a distinct Ca and Sr isotope compositions as a consequence of different physiochemical processes taking place in the subseafloor, such as conductive heating of seawater upon recharge of seawater into the hydrothermal system versus mixing of hydrothermal fluid and seawater. The anhydrite formed and recovered from the TAG MOR hydrothermal system, used in this study, is representative of the zone of anhydrite precipitation at and directly below the active sulfide mound at the seafloor, as a consequence of significant mixing of conductively heated seawater with high temperature end-member hydrothermal fluids.

(Schmitt et al., 2003). The Ca isotope data derived from TAG are also compared with previously measured stable O isotope, radiogenic Sr isotope, and fluid inclusion homogenization temperature data of anhydrite recovered from drill core from the TAG mound (Chiba et al., 1998; Humphris, 1998; Teagle et al., 1998a; Humphris and Bach, 2005). The experimental constraints applied to the natural anhydrite and hydrothermal fluid data provide a better understanding of Sr/Ca partitioning and Ca isotope fractionation systematics at MOR and volcanic arc hydrothermal systems.

2. METHODS

2.1. Experimental hydrothermal batch reactions

This study employs a novel experimental method utilizing flexible gold cell reactor technology coupled with the use of Ca isotopes as a tracer of reaction progress (Fig. 2) (Seyfried et al., 1987; Berndt et al., 1988; Beck et al., 1992). The experimental system, housed at the University of Minnesota, permits time-series sampling of reactor solution and injection of chemically anomalous solutions into

Please cite this article in press as: Syverson D. D., et al. Experimental partitioning of Ca isotopes and Sr into anhydrite: Consequences for the cycling of Ca and Sr in subseafloor mid-ocean ridge hydrothermal systems. *Geochim. Cosmochim. Acta* (2018), https://doi.org/10.1016/j.gca.2018.03.018

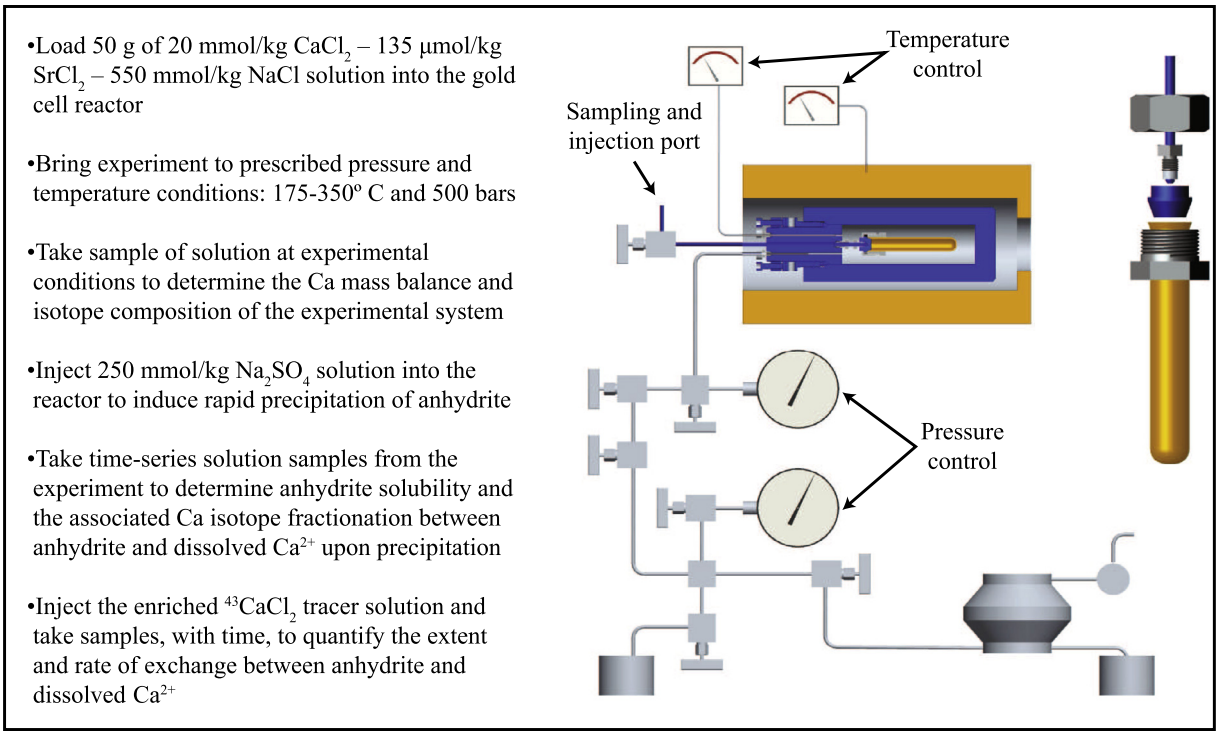

Fig. 2. Schematic diagram of the flexible gold reactor hydrothermal equipment and the experimental procedure used to induce anhydrite precipitation by addition of Na_2SO_4 solution into the $CaCl_2$-bearing reactor solution at experimental conditions. An enriched ^{43}Ca tracer solution was used after the anhydrite precipitation event to quantify the extent of exchange between anhydrite and dissolved constituents at experimental conditions. Sampling of the experimental solution and introduction of the Na_2SO_4 and ^{43}Ca enriched solution into the reactor solution occurred via the sampling and injection port by use of a high pressure ISCO™ pump (not shown).

the gold cell reactor at experimental conditions. Two different solutions were introduced into the experiment at desired temperature and pressure conditions: (1) a SO_4^{2-} bearing solution and (2) an enriched ^{43}Ca spike solution. The former is used to induce the precipitation of anhydrite from a $CaCl_2$-bearing solution, whereas the addition of the ^{43}Ca spike solution is used to quantify the extent and rate of isotope exchange between precipitated anhydrite and dissolved Ca reservoirs over the course of the experiment (Fig. 2).

Experiments are initiated at ambient conditions by addition of approximately 50 grams of synthetic Na–Ca–Sr–Cl solution of near seawater ionic strength composed of approximately 20 mmol/kg $CaCl_2$ – 135 µmol/kg $SrCl_2$ – 550 mmol/kg NaCl into the gold cell reactor, which is subsequently sealed (Table 1 and Fig. 2). The gold cell reactor assembly is then transferred and sealed into a steel autoclave pressure vessel, pressurized, and brought to the desired experimental temperature in a power-proportioning controlled furnace monitored by a Type K thermocouple in direct contact with the H_2O confining medium. The fluid in the gold cell reactor is sampled at each condition prior to anhydrite precipitation, at 175, 250, and 350 °C and 500 bars, to constrain the bulk chemical and Ca isotope composition of the experimental system (i.e. ΣCa and ΣSr). After the initial sampling, anhydrite precipitation commenced upon the metered delivery of approximately 5–7 g of 250 mmol/kg Na_2SO_4 solution (pH = 6.5). The added Na_2SO_4 solution was preceded and followed by injection of approximately 1 g of 550 mmol/kg NaCl solution to prevent anhydrite precipitation in the sampling tubing and to ensure quantitative delivery of the SO_4-bearing solution into the gold cell reactor, respectively. The amount of Na_2SO_4 solution injected into the gold cell reactor was designed such that approximately 30–40% of the total Ca remained in the fluid phase after the anhydrite precipitation event (Tables 1 and 2). The first solution sample after the onset of the anhydrite precipitation was typically taken within the first hour to track chemical and isotopic changes associated with the rapid precipitation of anhydrite. Sampling continued prior to the injection of the ^{43}Ca spike to further characterize Sr/Ca partitioning and fractionation of Ca isotopes during the initial period of recrystallization. After allowing for isotopic and elemental exchange between anhydrite and coexisting dissolved components to approach chemical saturation (Table 1 and Fig. 3), an anomalous solution enriched in ^{43}Ca was added to the contents of gold cell reactor by use of the high pressure ISCO pump, following similar procedures as previously described above for the Na_2SO_4 solution. Approximately 2–3 g of the ^{43}Ca isotope solution, with a $^{43}Ca/^{40}Ca$ ratio and Ca^{2+} concentration of 0.35 and 0.54 mmol/kg, respectively, were introduced to the experimental system, resulting in a mixed Ca isotope composition of the gold cell solution ranging between approximately 180 and 380‰, in δ-notation relative to the $^{43}Ca/^{40}Ca$ ratio of modern seawater (Tables 1 and 2). The

Please cite this article in press as: Syverson D. D., et al. Experimental partitioning of Ca isotopes and Sr into anhydrite: Consequences for the cycling of Ca and Sr in subseafloor mid-ocean ridge hydrothermal systems. *Geochim. Cosmochim. Acta* (2018), https://doi.org/10.1016/j.gca.2018.03.018

Please cite this article in press as: Syverson D. D., et al. Experimental partitioning of Ca isotopes and Sr into anhydrite: Consequences for the cycling of Ca and Sr in subseafloor mid-ocean ridge hydrothermal systems. *Geochim. Cosmochim. Acta* (2018), https://doi.org/10.1016/j.gca.2018.03.018

Table 1
Time-series solution samples and product anhydrite derived from the anhydrite precipitation and recrystallization experiments at 175, 250, and 350 °C and 500 bars.

Sample	Time (h)	$pH_{25°C}$	Soln. mass (g)	$[Ca^{2+}]$ (mM)	$[Sr^{2+}]$ (μM)	$[SO_4^{2-}]$ (mM)	$[Na^+]$ (mM)	$[Cl^-]$ (mM)	[a]K_D (Sr/Ca)	$\delta^{43}Ca$ (‰)	$\delta^{44}Ca$ (‰)	2σ (‰)
Expt. #1 175 °C												
Anh. 1-1	0	5.07	58.894	18.81	129	0.08	524	589	–	−0.55	−0.72	0.06
Anh. 1-2	1.2	5.33	52.104	16.11	107	15.52	505	544	1.24	−0.47	−0.61	0.04
Anh. 1-3	95	5.49	48.048	9.71	80	6.36	497	551	0.68	−0.30	−0.39	0.03
Anh. 1-4	647	5.49	45.292	9.88	83	4.03	501	530	0.64	−0.39	−0.51	0.04
[b]**Anh. 1-5**	669	5.46	42.478	9.52	80	3.93	515	529	0.65	[c]180.00	1.87	0.05
Anh. 1-6	691	5.56	45.598	10.00	83	4.00	525	529	0.65	175.85	1.36	0.08
Anh. 1-7	788	5.27	41.561	9.59	81	4.06	532	525	0.64	172.81	1.17	0.07
Anh. 1-8	978	5.26	38.903	9.79	82	4.02	524	525	0.64	171.14	1.36	0.13
Anh. 1-9	1365	5.47	35.625	9.77	83	4.23	519	528	0.62	167.93	1.25	0.09
Anh. 1-10	1991	5.30	32.729	9.75	82	4.13	522	530	0.65	165.47	1.19	0.07
Expt. #2 250 °C												
Anh. 2-1	0	5.43	54.301	19.12	132	0.03	522	566	–	−0.55	−0.72	0.08
Anh. 2-2	3.3	5.42	52.627	8.46	59	3.83	506	534	0.97	−0.41	−0.53	0.05
Anh. 2-3	11	5.34	48.936	7.73	64	0.91	529	535	0.72	−0.41	−0.54	0.07
Anh. 2-4	35	5.72	45.457	7.55	64	0.90	539	543	0.70	−0.38	−0.49	0.06
Anh. 2-5	323	5.82	42.561	7.41	65	0.89	524	530	0.66	−0.41	−0.53	0.09
[b]**Anh. 2-6**	325	5.63	41.674	6.96	65	0.87	520	528	0.60	[c]380.00	8.03	0.13
Anh. 2-7	327	5.82	38.216	6.98	65	0.90	516	528	0.60	378.83	3.15	0.09
Anh. 2-8	347	5.84	35.307	7.00	65	0.91	501	520	0.60	360.27	3.20	0.05
Anh. 2-9	448	5.88	33.090	6.81	67	0.85	505	511	0.55	316.12	2.31	0.12
Anh. 2-10	1192	5.84	30.123	6.95	67	0.92	511	521	0.54	243.54	1.96	0.08
Expt. #3 350 °C												
Anh. 3-1	0.0	6.12	44.718	20.81	148	0.01	591	643	–	−0.58	−0.75	0.05
Anh. 3-2	0.8	6.08	44.698	0.32	4.8	27.72	573	530	0.47	[c]n.a.	[c]n.a.	–
Anh. 3-3	2.7	5.80	42.316	1.27	19	1.09	580	600	0.45	[c]n.a.	[c]n.a.	–
Anh. 3-4	50	5.65	39.970	7.88	68	0.21	582	609	0.73	−0.52	−0.68	0.07
Anh. 3-5	68	5.57	38.343	8.09	70	0.18	585	616	0.71	−0.58	−0.75	0.03
[b]**Anh. 3-6**	70	5.50	38.403	7.74	67	0.20	583	610	0.72	[c]290.00	5.35	0.08
Anh. 3-7	74	5.62	36.551	7.84	68	0.23	583	611	0.72	285.44	5.27	0.11
Anh. 3-8	77	5.45	34.647	7.77	69	0.20	586	615	0.70	270.71	5.01	0.09
Anh. 3-9	96	5.58	32.575	7.77	70	0.18	586	612	0.68	258.85	4.77	0.13
Anh. 3-10	117	5.55	30.242	7.62	69	0.20	582	615	0.67	250.63	4.46	0.01
Anh. 3-11	172	5.62	27.827	7.64	71	0.16	581	606	0.65	232.92	3.99	0.05
Anh. 3-12	292	5.64	25.248	7.48	74	0.17	582	612	0.59	208.21	3.46	0.10
Anh. 3-13	436	5.52	22.031	7.43	77	0.17	582	613	0.55	188.94	3.35	0.07
Anh. Products	Time (hrs)		Sr/Ca (umol/mmol)						[d]K_D (Sr/Ca)	$\delta^{43}Ca$ (‰)	$\delta^{44}Ca$ (‰)	2σ (‰)
Anh-1	1991		5.55						0.66	2.03	−1.53	0.10
Anh-2	1192		5.30						0.55	30.73	−0.72	0.04
Anh-3	436		5.14						0.52	31.31	−0.25	0.05

The relative standard deviation (2σ) for the concentration of the individual dissolved components by ICP-OES and ion chromatography is ±2% for Na^+, ±1% for Ca and Sr, and ±1% for Cl^- and SO_4^{2-}. The solution mass reported is representative of the mass before each sampling event.

[a] The Sr/Ca partition coefficient, K_D, between anhydrite and dissolved constituents is calculated by mass balance of the time-series samples solution chemistry.

[b] The bold time-series solution samples, 1-5, 2-6, and 3-6, represent the initial sample taken after the ^{43}Ca spike injection, where the "time-zero" $\delta^{43}Ca$ isotope composition is calculated by linear extrapolation of the two following samples post-injection.

[c] The abbreviate, "n.a.", stands for "not analyzed" with respect to the Ca isotope composition of the solution sample. The Ca isotope samples are shown with the 2σ relative standard deviation. These specific samples were not analyzed as a result of low Ca/Na ratios due to mixing effects immediately after the Na_2SO_4 solution injection into the gold cell reactor solution.

[d] The directly measured K_D between product anhydrite and the final solution sample.

Table 2
^{43}Ca isotope exchange and rate systematics derived from the anhydrite-fluid exchange experiments.

Sample	[a]Time (h)	Solution mass (g)	$[Ca^{2+}]$	$\delta^{43}Ca$	2σ	$X_{Ca(Fluid)}$	[c]$\delta^{43}Ca$ (system)	[d]F (%)	[e]$ln[k(F)]$	[f]$K_{D(Equil.)}$ (Sr/Ca)
Expt. #1 175 °C										
Anh. 1-5	0	45.598	9.52	**180.00**	0.05	0.46	85.65	0.0		
Anh. 1-6	22	41.561	10.00	175.86	0.08	0.46	85.70	3.6		
Anh. 1-7	119	38.903	9.59	172.82	0.07	0.43	79.23	6.2		
Anh. 1-8	309	35.625	9.79	171.08	0.13	0.42	76.93	7.7		
Anh. 1-9	697	32.729	9.77	167.94	0.09	0.40	73.22	10.4		
Anh. 1-10	1322	30.583	9.75	165.48	0.07	0.38	70.35	12.5		
Anh. Prod. 1	1322	–	–	[b]1.96	0.06	0.38	[c]63.88	3.6	−13.67	0.43 ± 0.12
Expt. #2 250 °C										
Anh. 2-6	0	41.674	6.96	**380.00**	0.13	0.31	116.62	0.0		
Anh. 2-7	3	38.216	6.98	378.84	0.09	0.29	110.12	0.2		
Anh. 2-8	23	35.307	7.00	360.63	0.05	0.28	104.26	6.5		
Anh. 2-9	123	33.090	6.81	316.07	0.12	0.26	97.24	21.4		
Anh. 2-10	867	30.123	6.84	243.56	0.08	0.24	92.43	45.7		
Anh. Prod. 2	867	–	–	[b]30.72	0.05	0.24	[c]81.61	37.9	−12.10	0.34 ± 0.05
Expt. #3 350 °C										
Anh. 3-6	0.2	38.403	7.74	**290.00**	0.11	0.35	97.59	0.0		
Anh. 3-7	4.0	36.551	7.84	285.39	0.09	0.34	95.65	2.1		
Anh. 3-8	7.3	34.647	7.77	270.73	0.13	0.33	91.44	8.6		
Anh. 3-9	26	32.575	7.77	258.87	0.01	0.31	88.06	13.9		
Anh. 3-10	47	30.242	7.62	250.55	0.05	0.30	82.88	17.6		
Anh. 3-11	102	27.827	7.64	232.90	0.10	0.28	79.13	25.4		
Anh. 3-12	222	25.248	7.48	208.17	0.07	0.27	74.13	36.4		
Anh. 3-13	366	22.031	7.43	188.92	0.11	0.25	69.63	45.0		
Anh. Prod. 3	366	–	–	[b]31.25	0.03	0.23	[c]65.42	48.6	−11.14	0.29 ± 0.02

[a] The first spike sample, normalized at time zero, was taken approximately a half hour after the injection of the ^{43}Ca solution spike into the experimental solution. The concentration of dissolved Ca of the ^{43}Ca isotope spike solution is 0.54 mmol/kg and has a $^{43}Ca/^{40}Ca$ ratio of 0.35 whereas the natural $^{43}Ca/^{40}Ca$ ratio is ~0.001.

[b] The measured composition of product anhydrite recovered upon termination of the experiment. The mass of ^{43}Ca spike solution added to the gold cell reactor solution was approximately 1.5–2.5 g for each experiment. Before and after the spike injection, 1 g of 550 mmol/kg NaCl solution was added to effectively flush the Ti-capillary tubing free of experimental solution and ^{43}Ca spike, respectively.

[c] The directly measured composition of the system (anhydrite + dissolved Ca) at the termination of the experiment.

[d] F(%) is the fractional degree of Ca isotope exchange. The degree of exchange, F, for the final sample is determined by measuring the complete isotopic mass balance of the system, i.e. product anhydrite and the final solution sample.

[e] The rate of Ca isotope exchange between the anhydrite and fluid, $k(F)$, is determined by the best fit of a 1st order exchange model, where the units are in s^{-1}.

[f] Equilibrium estimate of the Sr/Ca partitioning between anhydrite and fluid, $K_{D(Equil.)}$, by use of the rate constant data from each experiment coupled with time-series changes in K_D (see text).

Please cite this article in press as: Syverson D. D., et al. Experimental partitioning of Ca isotopes and Sr into anhydrite: Consequences for the cycling of Ca and Sr in subseafloor mid-ocean ridge hydrothermal systems. *Geochim. Cosmochim. Acta* (2018), https://doi.org/10.1016/j.gca.2018.03.018

time-zero, $t = 0$, $\delta^{43}Ca$ composition for the exchange rate analysis was estimated by determination of the y-intercept by linear regression of the first three samples immediately after the injection of the ^{43}Ca spike solution into the reactor. Subsequently, time-series solution samples were taken to gauge the extent of exchange between anhydrite and dissolved Ca^{2+} that occurred upon recrystallization throughout the remainder of each experiment.

2.2. Major/minor element analyses

The time-series solution samples were retrieved in a syringe attached to a high pressure metering valve, where approximately 2–3 g of solution were allocated between bottles and diluted appropriately with de-ionized H_2O for anions and cations and for Ca isotope analysis. Prior to recovery of the solution sample used for chemical and isotopic analysis, a rinse sample (1 g) was taken to effectively flush the sampling tubing of residual fluid not indicative of the solution chemistry of the reactor solution at each time step. After completion of each experiment, the gold cell reactor assembly was quenched, within 30 min, to ambient temperature and pressure conditions and product anhydrite was immediately recovered, filtered, washed in de-ionized water, and allocated into bottles for cation/anion and Ca isotope analysis. The chemical components of sample solutions and product anhydrite were analyzed by ICP-OES and IC with a relative standard deviation (2σ) for ±2% for Na, Ca, and SO_4, ±1% for Cl, and ±4% for Sr.

2.3. Ca and Sr isotope analyses

The Ca and Sr isotope composition of naturally and experimentally derived solution and anhydrite samples were processed and analyzed by a Neptune Plus MC-ICP-MS at Princeton University. The anhydrite was initially digested in warm 0.5 N HNO_3 and evaporated to dryness and reconstituted in 2–3 mL of 0.5 N HNO_3. Samples for Ca and Sr isotope analyses were processed using an automated high-pressure ion chromatography (IC) system (Dionex ICS-5000+) following previously published methods (Fantle and Tipper, 2014; Blattler et al., 2015; Husson et al., 2015; Gothmann et al., 2016). Dissolved samples were analyzed for $\delta^{44/42}Ca$ and $\delta^{44/43}Ca$ values on a Thermo Scientific Neptune Plus MC-ICP-MS (Blattler and Higgins, 2014; Fantle and Higgins, 2014; Blattler et al., 2015; Husson et al., 2015; Gothmann et al., 2016). Measurements are carried out in medium resolution for Ca to avoid $ArHH^+$ interferences. All Ca isotope data are reported in delta notation relative to a known standard for Ca isotopes, seawater, and measured $\delta^{44/42}Ca$ values are converted to $\delta^{44/40}Ca$ values assuming mass-dependent fractionation with a slope of 2.05 and no excess radiogenic ^{40}Ca (Fantle and Tipper, 2014):

$$\delta^{x}Ca = \left[\frac{R^{x/40}}{R^{x/40}_{SW}} - 1\right](‰) \quad \text{where } x = 43 \text{ or } 44 \tag{1}$$

Although the Sr^{2+} is separated from Ca during ion chromatography, we correct for occasional small Sr^{2+} isobaric interferences in the Ca measurements using measurements at m/z = 43.5 (doubly-charged $^{87}Sr^{2+}$). All Ca isotope values are compared in three-isotope space ($\delta^{44/42}Ca$ vs. $\delta^{43/42}Ca$) to verify that the Ca isotope variability falls along the expected mass-dependent line (with the exception of samples containing the ^{43}Ca spike).

Sr isotope analyses of dissolved anhydrite were carried out at Princeton University on a Neptune MC-ICP-MS. Sr was separated from other matrix cations using a Dionex ICS-5000 + high-pressure IC system as described above. Sr isotope analyses by MC-ICP-MS follow previously published methods (Balcaen et al., 2005). The accuracy and precision of our analyses is determined by repeated chromatography and mass spectrometery of modern seawater ($^{87}Sr/^{86}Sr = 0.70918$, Faure and Mensing (2005)). Measured $^{87}Sr/^{86}Sr$ ratios of 8 seawater standards are 0.709188 ± 27 ppm (2σ). All Sr isotope data were normalized to the standard, NBS SRM987 ($^{87}Sr/^{86}Sr = 0.710248$), analyzed during the same analytical session.

Long-term external reproducibility for each isotopic system is determined based on the difference between two known standards taken through the full chemical procedure (column chromatography and mass spectrometry) with each batch of samples. For Ca isotopes we report external reproducibility using the measured value of SRM915b relative to modern seawater, both of which are processed and analyzed alongside a set of 20–30 samples on the same IC run. Our measured $\delta^{44/40}Ca$ value for SRM915b relative to modern seawater is −1.18 ± 0.16‰ (2σ, n = 125), indistinguishable from published values determined by both MC-ICP-MS and TIMS (Fantle and Tipper, 2014; Feng et al., 2017). All Ca isotope samples are reported relative to modern seawater ($\delta^{44}Ca_{seawater} = 0‰$). $\delta^{44}Ca_{seawater} = +1.92‰$ on the SRM915a scale and +0.98‰ on the bulk silicate Earth (BSE) scale (Fantle and Tipper, 2014). Reported errors for each sample depend on the number of times the sample has been separated and analyzed. For a single separation and analysis, we report the long-term external reproducibility of SRM915b or Cambridge-1 (2σ = ±0.16‰, and ±0.09‰, respectively). For multiple separations and analysis (N > 1) we also report the standard error of the mean (SE).

2.4. Sr/Ca partitioning in batch experiments

The Ca isotope data of anhydrite and dissolved Ca, together with time-series changes of dissolved Sr^{2+} can be used to determine if the observed Sr/Ca partition constant, K_D, is indicative of equilibrium, or if a steady-state has been achieved between dissolved Ca and Sr species and the bulk composition of coexisting anhydrite. At each experimental temperature. K_D is calculated as followed:

$$K_{D(Anh/Fluid)} = (X_{Sr}/X_{Ca})_{(Anh)}/([Sr]/[Ca])_{Fluid} \tag{2}$$

where $([Sr]/[Ca])_{Fluid}$ is the ratio of the measured concentration of dissolved Sr and Ca whereas $(X_{Sr}/X_{Ca})_{(Anh)}$ is the mole fraction ratio of Sr and Ca in anhydrite determined by mass balance by comparison of the experimental system solution chemistry relative to the time-series solution samples. Calculated activities of the solution species and for the dissolved components of anhydrite were not used for

Please cite this article in press as: Syverson D. D., et al. Experimental partitioning of Ca isotopes and Sr into anhydrite: Consequences for the cycling of Ca and Sr in subseafloor mid-ocean ridge hydrothermal systems. *Geochim. Cosmochim. Acta* (2018), https://doi.org/10.1016/j.gca.2018.03.018

this calculation to remain comparable with past experimental and natural studies.

At the termination of each experiment, the Sr/Ca concentration ratio and Ca isotope composition of the product anhydrite was compared with the final time-series solution sample to confirm that the experimental system fulfills elemental and isotope mass balance constraints. Finally, the experimental anhydrite product was analyzed by scanning electron microscopy (SEM) to characterize morphology after precipitation and recrystallization.

2.5. Ca isotope fractionation upon anhydrite precipitation

The fractionation of Ca isotopes between anhydrite and dissolved Ca^{2+} is reported as:

$$\Delta^x Ca_{[Anh-Ca(aq)]} = \delta^x Ca_{Anh} - \delta^x Ca_{(aq)} \quad (3)$$

where $x = 43$ or 44. The Ca isotope composition of anhydrite is determined through mass balance constraints imposed by the measured composition of the experimental components taking account of mass loss during fluid samples:

$$\delta^x Ca_{System} = X_{Anh}\delta^x Ca_{Anh} + X_{(aq)}\delta^x Ca_{(aq)} \quad (4)$$

where X is the mole fraction of Ca relative to each respective phase, anhydrite and dissolved Ca^{2+}. In addition, the fractionation between anhydrite and dissolved Ca^{2+} produced by rapid initial precipitation of anhydrite from solution is calculated through linear regression analysis using a Rayleigh fractionation model:

$$\ln(1000 + \delta^x Ca_{(aq)_f})/(1000 + \delta^x Ca_{t=0}) = \ln(f)(\alpha_{(Anh-Ca)} - 1) \quad (5)$$

where f is the fraction of Ca^{2+} remaining in solution, $\delta^x Ca_{(aq)_f}$ is the isotopic composition of the solution at each stage of f, and $\alpha_{(Anh-Ca)}$ is the associated fractionation produced between anhydrite and dissolved Ca^{2+} upon precipitation at each experimental condition. The Rayleigh fractionation model is appropriate to use during the precipitation event, since the rate of precipitation is rapid, and subsequent exchange between incipiently formed anhydrite and dissolved Ca^{2+} is limited.

2.6. Quantification of the extent and rate of anhydrite recrystallization using a ^{43}Ca spike

To quantify the extent of Ca isotope mixing, F, between anhydrite and coexisting dissolved constituents, we use the time-series solution Ca isotope data, δ^{43}_tCa, the time-zero isotopic composition immediately after the ^{43}Ca isotope injection, δ^{43}_0Ca, and the isotopic composition of the entire system (i.e. anhydrite + dissolved Ca^{2+}) measured at the termination of each experiment, $\delta^{43}_{\Sigma Ca}$Ca, as follows:

$$F = \frac{\delta^{43}_t Ca - \delta^{43}_0 Ca}{\delta^{43}_{\Sigma Ca} Ca - \delta^{43}_0 Ca} \quad (6)$$

Utilization of the bulk system Ca isotope composition, $\delta^{43}_{\Sigma Ca}$Ca, for the calculation of F is justified since the introduction of the ^{43}Ca spike into the reactor solution results in a highly anomalous initial δ^{43}Ca composition (>100‰), significantly larger in magnitude than the equilibrium fractionation expected upon complete exchange between anhydrite and dissolved Ca^{2+} (Johnson et al., 2004). The $\delta^{43}_{\Sigma Ca}$Ca determined at the end of the experiment was used since the Ca isotope composition of the system evolves upon sampling and removal of solution throughout reaction progress. In addition, mass-balance constraints between the Ca reservoirs, anhydrite and fluid, are utilized to quantify the relative amount of anhydrite recrystallized with time for each experiment, as described further by Handler et al. (2014):

$$F' = \frac{m^{Ca}_{Soln}[\delta^{43}_o Ca - \delta^{43}_t Ca]}{m^{Ca}_{Anh}[\delta^{43}_t Ca - \delta^{43}_{Anh} Ca]} \quad (7)$$

Specifically, the calculation of F' explicitly takes into account the relative mass balance of Ca in anhydrite and dissolved Ca reservoirs, where m^{Ca}_{Soln} and m^{Ca}_{Anh}, represent the total moles of Ca in solution and anhydrite, respectively.

Linear regression of the δ^{43}Ca fractional exchange, F, with time, t, is used to estimate the rate constant, k_{Anh} (s^{-1}), for Ca isotope exchange between anhydrite and dissolved Ca during recrystallization at each temperature. The time dependent isotope exchange data are applied to a first-order rate law (Cole et al., 1983, 1987, Criss et al., 1987; Gregory et al., 1989; Criss, 1999; Johnson et al., 2002):

$$ln(1 - F) = -k_{Anh}t \quad (8)$$

The first-order rate law was utilized since it provided a reasonable fit of the observed time-series δ^{43}Ca solution data and is comparable to previous experimentally determined exchange rate data based on ^{18}O isotope systematics between anhydrite and water (Chiba et al., 1981). The temperature dependence of the rate constant for Ca isotope exchange, k_{Anh}, is quantified by determination of the activation energy, E_A, where T is in Kelvin, R is the gas constant, and $\ln(A')$ is the pre-exponential factor which describes the frequency of molecular collisions:

$$ln(k_{Anh}) = (-E_A/R) * (10^3/T) + ln(A') \quad (9)$$

With this specific Ca isotope exchange rate data, the degree and mechanism of exchange can be estimated for a range of hydrothermal conditions indicative of subseafloor hydrothermal systems, providing information fundamental to the interpretation of the Ca and Sr elemental/isotopic composition of natural hydrothermal fluids and anhydrite.

2.7. Geochemical modeling and speciation calculations

The saturation state of the batch experiments with respect to anhydrite was determined using the thermodynamic modeling software, Geochemist's Workbench (Bethke, 2006). Model inputs include measured concentrations of the dissolved components, Ca^{2+}, Sr^{2+}, Na^+, Cl^-, SO_4^{2-} and pH at 25 °C. A modified equilibrium database, required for the thermodynamic model to determine the

Please cite this article in press as: Syverson D. D., et al. Experimental partitioning of Ca isotopes and Sr into anhydrite: Consequences for the cycling of Ca and Sr in subseafloor mid-ocean ridge hydrothermal systems. *Geochim. Cosmochim. Acta* (2018), https://doi.org/10.1016/j.gca.2018.03.018

speciation of aqueous species was created by the DBCreate program developed by Kong et al. (2013) for the range of temperatures and pressure considered in this study, 25–400 °C and 500 bars. The algorithms required for the derivation of the thermodynamic data are consistent with Helgeson-Kirkham-Flowers equation of state and complementary revisions (Helgeson et al., 1981; Tanger and Helgeson, 1988; Shock et al., 1989, 1992, 1997; Sverjensky et al., 1997). The thermodynamic model assumes the activity of water and anhydrite is unity and the associated activity coefficients for charged dissolved species are approximated by the extended Debye-Hückel equation. The assumption of unity for the activity of water is justified since explicit calculation of the activity of water at experimental P-T-X conditions indicate a range in activity between 0.98 and 0.99 (Archer, 1992). The thermodynamic model takes advantage of the appropriate mass balance, mass action, and charge balance constraints coupled with the measured composition of the time-series solution samples to determine the distribution and speciation of dissolved constituents and mineral stability at experimental conditions (Fig. 3).

2.8. Natural analogue - TAG hydrothermal system

The TAG hydrothermal system, located at 26°08′N along a slow-spreading segment of the Mid-Atlantic Ridge, is a massive sulfide deposit that has been episodically active for over 20,000 years (You and Bickle, 1998). Since the discovery of high temperature vents at TAG in 1985, it has served as an important site for better understanding the geochemical, geophysical, and biological characteristics of active massive sulfide deposits at and below the seafloor of MOR hydrothermal systems (Rona et al., 1986; Humphris et al., 2015). TAG is particularly relevant to this study as drill cores from the massive sulfide mound of this site, recovered from ODP Leg 158, contain abundant anhydrite and there is extensive geochemical evidence that conductive heating and mixing of seawater with high temperature hydrothermal fluids play a key role controlling anhydrite formation (e.g. SF:HF mixing zone of Fig. 1) (Humphris et al., 1995; Herzig et al., 1998; Mills et al., 1998; Teagle et al., 1998a). This is confirmed by anhydrite fluid inclusion data and the intermediate Sr isotope composition of anhydrite relative to MORB and seawater (Petersen et al., 1998; Tivey et al., 1998). In addition, high temperature vent fluids (>350 °C) at TAG have recently been sampled, adding chemical and isotopic data with which the experimental data reported here can be compared.

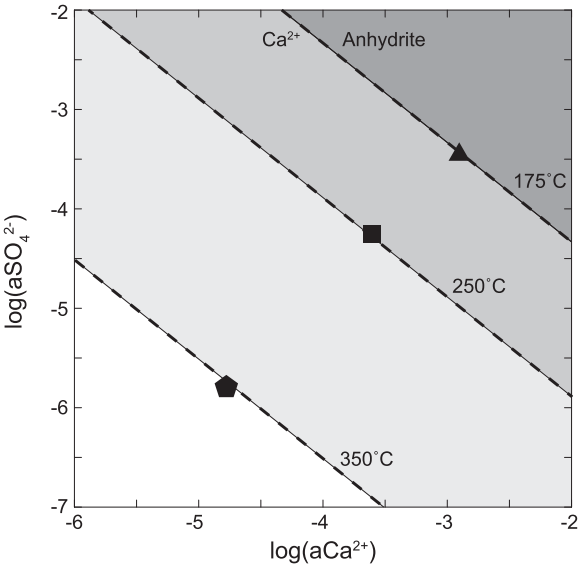

Fig. 3. Aqueous activity diagram depicting theoretically predicted anhydrite solubility in comparison with the speciated composition of experimental fluids where the triangle, square, and the pentagon represent experiments at 175, 250, and 350 °C, respectively. The observed solubility data demonstrates that the experimental system is at chemical equilibrium, after the precipitation event, with respect to anhydrite-fluid solubility at the prescribed pressure and temperature conditions. The symbols, for each temperature, represent the average activity of SO_4 and Ca determined from all samples taken after the precipitation event. The deviation amongst time-series samples and the uncertainty in the speciated activity is approximately the size of each symbol.

The anhydrite samples collected from the TAG hydrothermal vent system are taken from a core drilled on a sulfide mound on IODP Leg 158 and contains sulfide/anhydrite stock-work as described by Humphris et al. (1995). The anhydrite collected for Ca isotope analysis is from the drill core half, 158-957C-7N-2, recovered from the depth interval of 20.25–20.31 m below the seafloor (Table 3). Anhydrite sampled from the same approximate depth and interval of the core half, 158-957C-7N-1, which has previously been analyzed for $\delta^{18}O$, $\delta^{34}S$, $^{87}Sr/^{86}Sr$, and fluid inclusion homogenization temperatures, are used for comparison with this study (Chiba et al., 1998; Mills et al., 1998; Teagle et al., 1998a; Tivey et al., 1998; Mills and Tivey, 1999).

The high temperature vent fluids at TAG were retrieved by use of the remotely operated vehicle, JASON II, during a scientific expedition in 2008 aboard R/V Roger Revelle (KNOX18RR). The procedure for sampling the high-temperature solution was facilitated by use of a gas-tight Ti-sampler system, which is aided by a thermocouple to guide the sampler snorkel into the highest temperature fluid issuing from the sulfide mound, minimizing mixing of seawater with the hydrothermal fluid during sampling (Seewald et al., 2001; Wu et al., 2011). The sampled hydrothermal fluid is subsequently brought aboard ship, typically within a few hours, and allocated into acid-washed polyethylene bottles for cation, anion, and isotope analysis (Table 3). An aliquot of the sampled hydrothermal solution was measured for pH by use of a Ross micro-electrode, which was calibrated with pH buffers of 4, 7, and 10. The solution samples for cations and anions were diluted with 0.1 N ultra-trace metal grade HCl and deionized water, respectively, and preserved for analysis by IC and ICP-OES at the University of Minnesota. The uncertainties associated with the chemical and isotopic analysis of the hydrothermal fluids are analogous to those described for the measurements of the experimental samples.

Please cite this article in press as: Syverson D. D., et al. Experimental partitioning of Ca isotopes and Sr into anhydrite: Consequences for the cycling of Ca and Sr in subseafloor mid-ocean ridge hydrothermal systems. *Geochim. Cosmochim. Acta* (2018), https://doi.org/10.1016/j.gca.2018.03.018

Table 3
Hydrothermal fluid samples and anhydrite sampled from the TAG hydrothermal vent field along the Mid-Atlantic Ridge.

TAG fluid samples	Temp. (°C)	$pH_{25°C}$	$[Mg^{2+}]$ (mM)	$[Ca^{2+}]$ (mM)	$[Sr^{2+}]$ (μM)	$[Na^{+}]$ (mM)	$[Cl^{-}]$ (mM)	$^{87}Sr/^{86}Sr$	$\delta^{43}Ca$ (‰)	$\delta^{44}Ca$ (‰)	2σ (‰)
Seawater	2	8	53.3	10.4	86	468	546	[a]0.70918		0	0.05
Kremlin (363-IGT4)	140	5.83	32.3	22.8	101	510	592	n.a.	−0.74	−0.99	0.05
Complex (363-CGT-R)	363	4.09	5.9	35.3	112	555	649	n.a.	−0.80	−1.02	0.04
Complex (363-IGT5)	363	3.28	3.9	39.4	126	552	646	n.a.	−0.91	−1.21	0.07
[b,c]End-member	–	–	0	40.2	123	563	658	[a] 0.70380	−0.90	−1.19	0.12
TAG anhydrite	Depth (mbsf)							[d] $^{87}Sr/^{86}Sr$	$\delta^{43}Ca$ (‰)	$\delta^{44}Ca$ (‰)	2σ (‰)
158-957C-7N-2-25 cm	20.25							0.707166	−0.81	−1.03	0.02
158-957C-7N-2-31 cm	20.31							0.707208	−0.86	−1.12	0.04
Anhydrite-fluid	[e]$\delta^{44}Ca_{HF:SW}$ (‰)	2σ (‰)	[e]$\Delta^{44}Ca_{Anh/Fluid}$ (‰)		2σ (‰)						
158-957C-7N-2-25 cm	−0.71	0.10	−0.32		0.10						
158-957C-7N-2-31 cm	−0.71	0.10	−0.42		0.10						

All concentrations are represented in mmol/kg solution. The relative standard deviation (2σ) for the concentration of the individual dissolved components by ICP-OES and ion chromatography is ±2% for Na^{+}, ±1% for Ca and Sr and ±1% for Cl^{-} and SO_4^{2-}.

[a] The radiogenic Sr data are derived from Edmond et al. (1995) with an average 2σ error associated of ±0.000010. The solution mass reported is representative of the mass before each sampling event.

[b] The end-member hydrothermal composition of the fluid sampled from TAG is determined from linear regression of Mg/Ca versus the $\delta^{44}Ca$ of seawater and sampled high-temperature fluid.

[c] The end-member Ca isotope composition of the hydrothermal fluid sampled from TAG is determined by linear regression of Mg/Ca versus the $\delta^{44}Ca$ of seawater and sampled high-temperature fluid.

[d] The measured $^{87}Sr/^{86}Sr$ ratio and fluid inclusion homogenization temperatures for sampled TAG anhydrite in this study is comparable in composition from the same section and depth of core previously reported by Mills and Tivey (1999) and Teagle et al. (1998a,b), 158-957C-7N-1.

[e] The fractionation between anhydrite and fluid, $\Delta^{44}Ca_{Anh/Fluid}$, is calculated from the Ca isotope composition of sampled anhydrite and the seawater/hydrothermal fluid mixture, from which it formed from, where the seawater/hydrothermal fluid Ca isotope composition was calculated through conservative mixing relationships, based on the $^{87}Sr/^{86}Sr$ and Ca isotope composition of anhydrite relative to seawater and hydrothermal fluid.

Please cite this article in press as: Syverson D. D., et al. Experimental partitioning of Ca isotopes and Sr into anhydrite: Consequences for the cycling of Ca and Sr in subseafloor mid-ocean ridge hydrothermal systems. *Geochim. Cosmochim. Acta* (2018), https://doi.org/10.1016/j.gca.2018.03.018

3. RESULTS

3.1. Experimental precipitation and recrystallization of anhydrite at 175, 250, and 350 °C

3.1.1. Major element chemistry and petrography of synthesized anhydrite

Over the first hours of the experiment, dissolved Ca and Sr concentrations decline by approximately 30–40% due to the formation of anhydrite as a result of the addition of the Na_2SO_4 solution into the gold cell reactor (Table 1). Dissolved SO_4 concentrations in each experiment increase over the same time interval from effectively zero to peak values during the initial mixing stage of the reaction, 3.83–27.72 mmol/kg. Subsequently, SO_4^{2-} concentrations decline, stabilizing at concentrations ranging from approximately 0.2 to 4 mmol/kg for the duration of the experiments. Dissolved Ca concentrations exhibit more complex behavior owing to the addition of the Na_2SO_4 and subsequent temperature dependent mixing and precipitation reactions. For example, dissolved Ca slowly declines at both 175 and 250 °C, but increases in the 350 °C experiment; however, all experiments eventually stabilize to values between approximately 7–10 mmol/kg Ca^{2+}. Thermodynamic speciation calculations for all time-series solution samples after the precipitation event are at saturation with respect to anhydrite solubility at each prescribed pressure and temperature (Fig. 3). For the entirety of each experiment, all sampled solutions had a measured pH at 25 °C between 5.26 and 5.84, whereas the range in pH at experimental conditions is between 5.30 and 5.50. In addition, all speciation calculation of the time-series solution samples from each experiment confirm that Sr-bearing minerals, such as strontianite ($SrCO_3$) and celestite ($SrSO_4$), are undersaturated.

SEM imaging indicates that product anhydrite at 350 °C has an acicular morphology, indicative of fast precipitation rates, as demonstrated by a previous experimental examination of anhydrite precipitation at hydrothermal conditions by Shikazono and Holland (1983) (Fig. 4). The range in grain size for product anhydrite, precipitated and recrystallized at 350 °C, is approximately between 300 and 10 μm. Furthermore, the large grain size distribution, suggests that the mechanism of recrystallization is a favorable process that effectively facilitates anhydrite growth and exchange between the mineral and fluid elemental and isotopic reservoirs (Dubinina and Lakshtanov, 1997). Although not shown here, the morphology of anhydrite from experiments at 175 and 250 °C is also acicular in morphology with a similar grain size distribution. The anhydrite crystals were not tested for chemical heterogeneity, and thus, are assumed to be unzoned.

3.1.2. Sr/Ca partitioning during precipitation and recrystallization of anhydrite

The Sr/Ca partition coefficient for anhydrite-fluid (K_D), calculated for each sample indicates that the initial precipitation event is predominantly associated with elevated K_D values, 1.24, 0.97, 0.73, for 175, 250, and 350 °C, respectively, relative to long-term K_D values (Table 1 and Fig. 5). Time evolution paths of K_D and the rate of approach to steady state, however, differ for each temperature as anhydrite undergoes recrystallization. For example, at 175 °C, K_D data reaches a steady state value of 0.68, 95 h after the precipitation event and little change occurs subsequently in the course of 1991 h. However, at higher temperatures, 250 and 350 °C, the time-series K_D data continue to evolve towards lower values, ultimately 0.56 and 0.55, throughout the course of each experiment, 1192 and 436

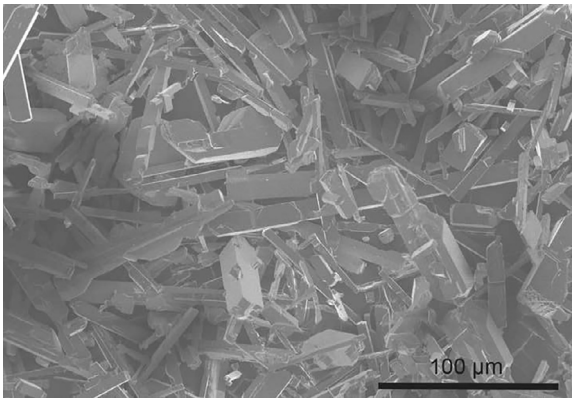

Fig. 4. SEM image of product anhydrite precipitated and recrystallized at 350 °C throughout the course of the 366 h experiment. The product anhydrite exhibits crystalline acicular morphology and a range in grain size, suggesting that the mechanism of recrystallization was likely the dominant process that facilitated exchange between the mineral and fluid elemental and isotopic reservoirs. The acicular morphology and similar size distribution of product anhydrite is also demonstrated for the lower temperature experiments at 175 and 250 °C (not shown).

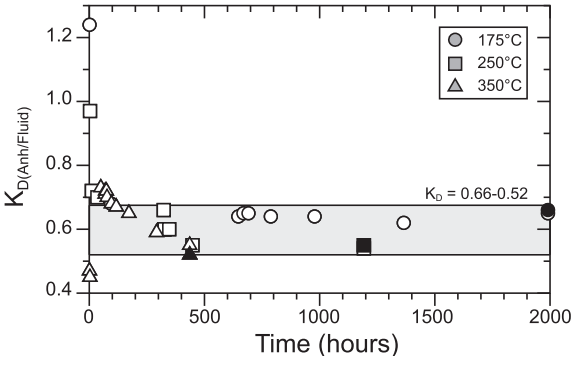

Fig. 5. Evolution of Sr/Ca partitioning, K_D, between anhydrite and dissolved Ca and Sr with reaction progress. Results based on mass calculations from solution chemistry (open symbols) and from the terminal measured compositions of anhydrite and dissolved Ca and Sr at the end of each experiment (black symbols). The calculated K_D values from the solution chemistry of early samples tend to exhibit relatively large range of values, approximately between 0.4 and 1.3 (see text). With increasing extents of anhydrite recrystallization with time the K_D values, from the perspective of solution chemistry, converge towards 0.65, 0.54, and 0.55 whereas the directly measured K_D from product anhydrite and the final solution sample have similar values, 0.66, 0.55, 0.52 for 175, 250, and 350 °C, respectively. The close agreement between the calculated and measured terminal K_D values demonstrates that the experimental system fulfills elemental mass balance constraints.

h, respectively. At the end of each experiment, the measured Sr/Ca ratio of product anhydrite was compared with the terminal solution sample, resulting in K_D of 0.66, 0.55, and 0.52 for 175, 250, and 350 °C, respectively, similar to that calculated from solution chemistry, confirming that mass balance was maintained throughout each experiment.

3.1.3. Fractionation of natural abundance Ca isotopes during anhydrite precipitation

For each experiment, prior to anhydrite precipitation, the natural Ca isotope composition of the initial solution sample was measured to constrain the initial Ca concentration and isotope composition of the experimental system prior to the addition of the ^{43}Ca isotope spike into the system, $\delta^{43,44}_{\Sigma Ca}$Ca, where δ^{43}Ca = −0.55 to −0.58‰ and δ^{44}Ca = −0.72 to −0.75‰ (Table 1). Upon precipitation of anhydrite, dissolved Ca declines but becomes concentrated in heavy isotopes due to Rayleigh-type distillation. By utilization of a Rayleigh fractionation model with the time-series solution chemistry and associated Ca isotope data (Eq. (5)), precipitation induced fractionation yields values of −0.45, −0.22, and −0.02‰, for 175, 250, and 350 °C, respectively (Fig. 6). These data demonstrate a clear temperature dependent fractionation trend, which is consistent with natural anhydrite-fluid fractionation data reported for the Logatchev hydrothermal system and from past low temperature experimental studies (Hensley and MacDougall, 2003; Amini et al., 2008; Blattler and Higgins, 2014). Although this result is consistent with predictions for equilibrium isotope effects, the inference of equilibrium requires independent confirmation through additional experiments which utilize three-isotope and partial exchange methods to ascertain between kinetic and equilibrium effects during rapid precipitation of anhydrite.

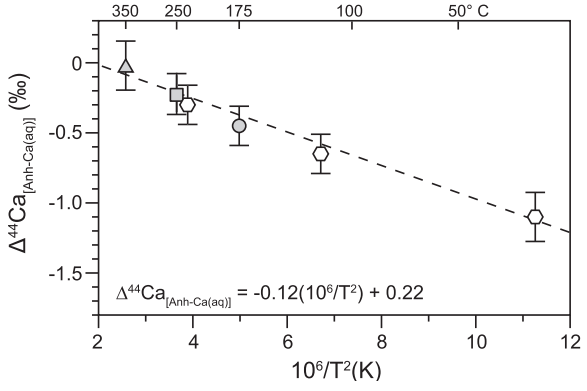

Fig. 6. Experimental and naturally observed δ^{44}Ca fractionation data between dissolved anhydrite and dissolved Ca^{2+}, $\Delta^{44}Ca_{[Anh\text{-}Ca(aq)]}$, as a function of temperature. The experimental data derived from this study at 175, 250, and 350 °C are represented as a grey circle, square, and triangle, respectively. The experimental fractionation data are determined by a Rayleigh fractionation model of the solution chemistry data after the precipitation event. The open hexagons represent δ^{44}Ca fractionation data derived from natural anhydrite and vent fluid sampled from the Logatchev hydrothermal field along the Mid-Atlantic Ridge reported by Amini et al. (2008) and from experimental samples of anhydrite and dissolved Ca^{2+} produced from evaporation experiments performed at 40 °C by Hensley and MacDougall (2003). The dashed line represents the temperature dependent δ^{44}Ca fractionation between Ca^{2+} and anhydrite determined from this study. All errors reported are representative of 2σ uncertainty. It must be noted that in spite of the strong correlation of fractionation versus temperature, the trend should be treated with caution when interpreting equilibrium versus kinetic effects since further experimental data are needed to justify these inferences.

3.1.4. Rates of anhydrite-dissolved Ca exchange at 175, 250, and 350 °C

After sufficient time was allowed for anhydrite to recrystallize and for the solution chemistry to reach chemical saturation conditions, an anomalous ^{43}Ca solution was introduced to quantify the rate of exchange at each temperature. The time of injection is normalized as $t = 0$. The time-zero dissolved δ^{43}Ca composition sampled following injection was determined from linear extrapolation of the first three anomalous δ^{43}Ca samples, resulting in 180, 380, and 290‰ for the experiments at 175, 250, and 350 °C, respectively (Tables 1 and 2). This extrapolation procedure was conducted to prevent sampling of mixing effects effectively after the injection of the anomalous ^{43}Ca solution into the gold cell reactor. As expected, with increasing recrystallization, the anomalous ^{43}Ca tracer decreases. The fraction of isotopic mixing between anhydrite and dissolved Ca^{2+}, F (calculated from the time-series Ca isotope composition) indicates that 13, 46, and 45% of the enriched ^{43}Ca tracer in solution exchanged with anhydrite at 175, 250, and 350 °C in the course of 1322, 867, and 366 h, respectively (Eq. (6), Table 2, and Figs. 7 and 8). Comparison of the calculated initial Ca isotope composition of

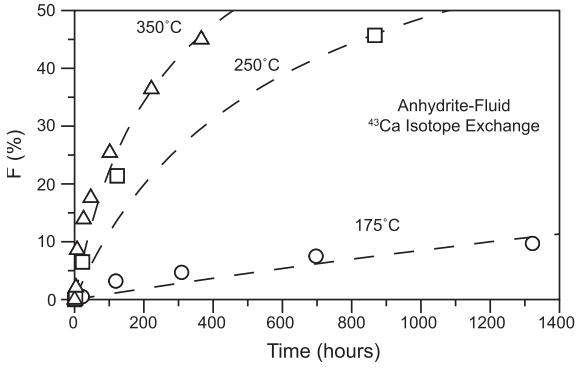

Fig. 7. Mixing between the Ca isotope reservoirs, anhydrite and dissolved Ca^{2+} (F), with time, where isotopic exchange is facilitated by hydrothermal recrystallization of anhydrite. F is determined by the change in the anomalous δ^{43}Ca isotope composition of the solution with time upon exchange with the natural Ca isotope reservoir of anhydrite. The times-series data indicate that the degree of exchange between the mineral-fluid reservoirs becomes more efficient at increasingly elevated temperatures, approximately 10, 46, and 45% exchange occurs within 1322, 867, and 366 h at 175, 250, and 350 °C, respectively. The dashed line extrapolation is determined by calculation of the rate constant for each temperature by implementing a 1st order rate model. It is important to note that each experiment from this study was designed, by mass balance, to be comparable to each other.

Please cite this article in press as: Syverson D. D., et al. Experimental partitioning of Ca isotopes and Sr into anhydrite: Consequences for the cycling of Ca and Sr in subseafloor mid-ocean ridge hydrothermal systems. *Geochim. Cosmochim. Acta* (2018), https://doi.org/10.1016/j.gca.2018.03.018

anhydrite, prior to the spike, with that of the isotopically enriched anhydrite at the end of the experiment indicates that 4, 38, and 49% mixing occurred at 175, 250, and 350 °C, respectively. The difference between the calculated degree of mixing, F, from the perspective of either Ca isotope reservoir, dissolved Ca^{2+} versus anhydrite, likely results from partial dissolution of product anhydrite during quench towards ambient conditions at the end of the experiment, since anhydrite becomes increasingly more soluble at lower temperature. As the reactor system allows sampling of the solution at experimental pressure and temperature conditions, estimated values of F from the time-series solution data are likely more accurate. The fraction of moles of Ca derived from anhydrite, *F'* (Eq. (7)), to effectively cause the observed change in the time-series $\delta^{43}Ca$ solution data, F (Eq. (6)), requires approximately 6, 18, and 15% of Ca exchanged from anhydrite upon recrystallization at 175, 250, and 350 °C throughout the course of 1322, 867, and 366 h, respectively.

Measured rates of chemical exchange between anhydrite and fluid are a strong function of temperature and similar in magnitude to those observed in previous experimental studies utilizing ^{18}O spikes to quantify the equilibration rate between anhydrite derived SO_4 and H_2O at hydrothermal conditions (Figs. 7 and 8) (Chiba et al., 1981). Linear regression of the rate constants derived from the Ca isotope exchange rate data, F, between anhydrite and dissolved Ca^{2+} at each experimental temperature (Table 2 and Fig. 7), yield an activation energy of 46 kJ/mol, a value that is also similar to that determined by Chiba et al. (1981). This range in magnitude of E_A is indicative of exchange

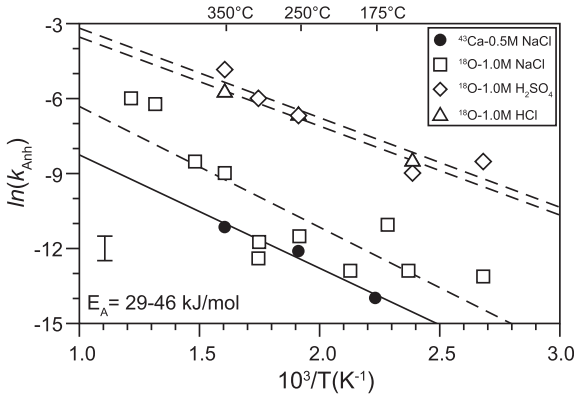

Fig. 8. The natural log of the rate constants, $ln(k_{Anh})$, in units of reciprocal time (s^{-1}), as a function of temperature. The $ln(k_{Anh})$ data are determined by linear regression of the fractional approach to complete mixing versus time by utilization of 1st order rate law (Table 2). The activation energy, E_A, indicative of Ca isotope exchange between anhydrite and dissolved Ca^{2+} at hydrothermal conditions is determined from the slope of the linear regression of the $ln(k_{Anh})$ data versus $10^3/T(K)$, amounting to approximately 46 kJ/mol. The magnitude of the E_A is consistent in magnitude with the exchange mechanism of dissolution and precipitation (i.e. recrystallization) and with previously calculated activation energies for oxygen isotope exchange reactions between sulfate minerals and dissolved constituents at similar experimental conditions, 29–46 kJ/mol (Chiba et al., 1981).

by dissolution and precipitation, where diffusion in anhydrite is likely the rate limiting effect on complete equilibration between anhydrite and dissolved constituents (Cole et al., 1983, 1987). In addition, Chiba et al. (1981) also noted that solution chemistry may impart a control on the rate of exchange, where fluids with a high H^+ activity, such as 1 M H_2SO_4 and 1 M HCl experimental solutions shown in Fig. 8, exhibit a lower activation energy, 29 kJ/mol, and thus, faster rates of exchange relative to experiments implementing circum-neutral fluids in NaCl solutions, 0.5 and 1.0 M, 42–46 kJ/mol. Furthermore, the rate data from experiments utilizing 0.5–1.0 M solutions, despite the small difference, suggests that an increase in the activity of Cl^- in solution, which effectively enhances the solubility of anhydrite by increasing the abundance of dissolved Ca–Cl complexes, may also increase the rate of elemental and isotopic exchange between anhydrite and the dissolved constituents in solution.

3.1.5. Equilibrium K_D values between anhydrite-fluid

To differentiate between equilibrium and kinetic K_D values, the rate constants derived from the ^{43}Ca exchange data were used. This allowed the determination of the equilibrium K_D value in spite of incomplete exchange, by linear regression of the entire dataset of time-series K_D values against the predicted degree of mixing with time, F (Fig. 9). This approach, however, does not use the initial K_D values produced during the rapid anhydrite precipitation event, which are indicative of kinetic and mixing effects. Equilibrium K_D values, as determined from the linear regression of the time series data at each temperature, indicate a slight, but significant temperature effect, as follows: 0.43 ± 0.12, 0.34 ± 0.05, 0.29 ± 0.02 (1σ), for 175, 250, and 350 °C, respectively. Despite the large error associated with 175 °C experiment, due to the limited amount of exchange between anhydrite and fluid throughout the experiment, the equilibrium K_D values throughout the range of temperatures are of the same relative magnitude with the K_D values demonstrated from near equilibrium anhydrite precipitation experiments at 150–250 °C, 0.31–0.21, by Shikazono and Holland (1983), and estimated by comparison of natural anhydrite and hydrothermal fluids from a range of MOR hydrothermal vent sites, 0.60 ± 0.28, as determined by Teagle et al. (1998a). This approach of estimating equilibrium partitioning values by utilization of exchange rate data for Ca and extrapolation to complete exchange is valid since Sr is intimately associated with Ca and that SO_4 and Ca exchange congruently, as evidenced by the similar time scales at which these components exchange with anhydrite (Chiba et al., 1981) Fig. 8.

3.2. Ca and Sr Chemical and Isotopic Systematics from the TAG hydrothermal vent field

Hydrothermal fluids from TAG were derived from both diffuse and focused-flow structures, having temperatures of approximately 140 and 363 °C, respectively (Table 3). The chemical composition of the diffuse flow fluid is relatively seawater-like, as indicated by the high Mg^{2+} concentration. As noted above these fluids have undergone conductive

Please cite this article in press as: Syverson D. D., et al. Experimental partitioning of Ca isotopes and Sr into anhydrite: Consequences for the cycling of Ca and Sr in subseafloor mid-ocean ridge hydrothermal systems. *Geochim. Cosmochim. Acta* (2018), https://doi.org/10.1016/j.gca.2018.03.018

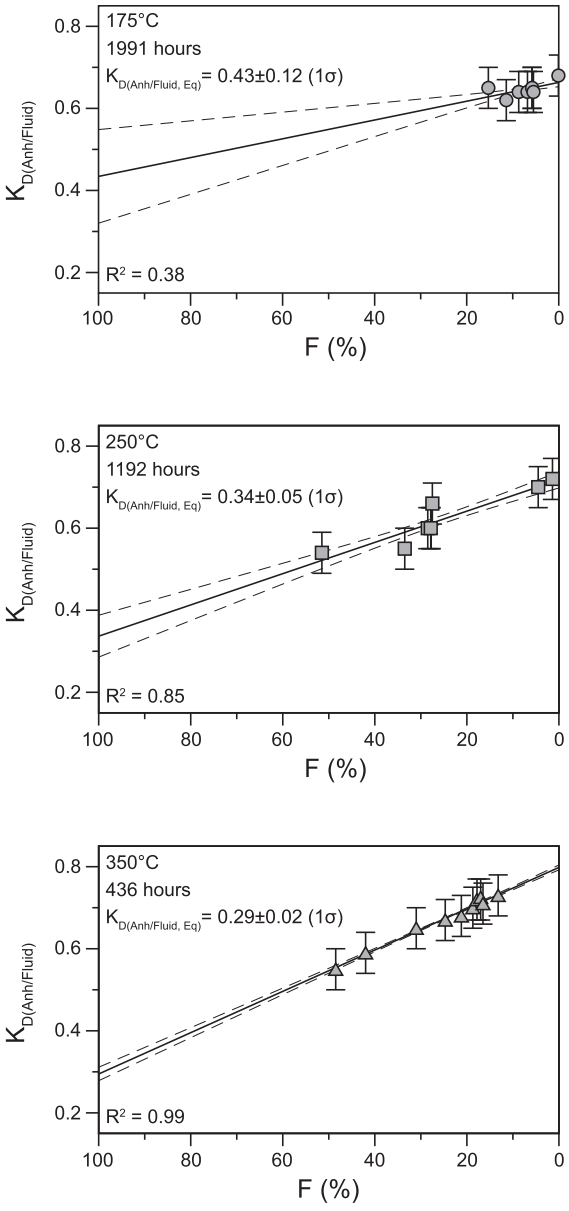

Fig. 9. Calculation of the equilibrium Sr/Ca partitioning coefficient between anhydrite and fluid, K_D, by extrapolation towards equilibrium, at 100% mixing, by utilization of rate constant data derived at each experimental temperature, 175, 250, and 350 °C. The extrapolation method regressed the experimental time-series K_D values at each temperature in conjunction with the exchange rate data determined upon recrystallization throughout the duration of each experiment; the initial K_D values, produced upon precipitation, were not used since these data are not representative of chemical effects indicative of anhydrite recrystallization at saturation. The equilibrium K_D values determined are 0.43, 0.34, and 0.29 at 175, 250, and 350 °C, respectively.

heating prior to seawater mixing. Evidence for this mixing includes elevated concentrations of dissolved Ca^{2+} and intermediate radiogenic Sr isotope composition between seawater and MORB, which is consistent with elevated homogenization temperatures in the subseafloor as determined from fluid inclusion analysis of anhydrite sampled from this same locality (Edmond et al., 1995; Tivey et al., 1995; Petersen et al., 1998; Teagle et al., 1998a). In contrast, the higher temperature vent fluids are typical of end-member hydrothermal fluids, which have near-zero dissolved Mg^{2+}. Multiple hydrothermal fluid samples were recovered such that the calculation of end-member elemental concentration and Ca isotope compositional data could be determined. Thus, extrapolation of the Ca^{2+} and Sr^{2+} compositional data from all of the sampled hydrothermal fluids, together, towards zero Mg^{2+} indicates that the estimated end-member hydrothermal fluid is composed of 40.2 mmol/kg Ca^{2+} and 123 μmol/kg Sr^{2+}, respectively. These data are similar to earlier reported data from TAG (Edmond et al., 1995; Rona et al., 1986). Following the same extrapolation procedure and assuming a $\delta^{44}Ca$ value for seawater of 0‰, end-member $\delta^{44}Ca$ value for the TAG hydrothermal fluid is estimated to be -1.19 ± 0.12‰ (2σ), approximately 0.0–0.2‰ lower than the measured $\delta^{44}Ca$ value of the sampled TAG hydrothermal fluid at the seafloor and 0.2‰ lower than average MORB (-1.02 ± 0.18‰, 2σ) (Feng et al., 2017).

The $\delta^{44}Ca$ value of the anhydrite samples are -1.03 ± 0.02 and -1.12 ± 0.04‰ (2σ), for core sections 158-957C-7N-2-25 cm and 158-957C-7N-2-31 cm, respectively (Table 3). The measured $^{87}Sr/^{86}Sr$ composition of anhydrite is 0.707166 and 0.707208, for 158-957C-7N-2-25 cm and 158-957C-7N-2-31 cm, respectively, similar in composition of anhydrite measured from the same depth interval of complementary drill core, 0.707102, by Teagle et al. (1998a).

By pairing of the $^{87}Sr/^{86}Sr$ and Ca isotope compositional data of anhydrite, seawater, and end-member hydrothermal fluid composition through conservative mixing relationships, the Ca isotope composition of the chemically evolved fluid (hydrothermal fluid + seawater) from which anhydrite precipitated directly can be estimated. Coupling of these specific data result in an average $\delta^{44}Ca$ composition of the evolved fluid from TAG, -0.71 ± 0.07‰ (2σ), where the $\delta^{44}Ca$ fractionation between anhydrite and evolved fluid, $\Delta^{44}Ca_{[Anh-Ca(aq)]}$, is calculated to be −0.32 and -0.42 ± 0.10‰ (2σ). These values are similar in sign and magnitude with past field data from Logatchev, shown by Amini et al. (2008), -0.33 ± 0.16 and -0.62 ± 0.09‰ (2σ), and with the experimental fractionation data reported from this study (Fig. 6).

4. DISCUSSION

4.1. Role of anhydrite in ocean hydrothermal environments and seawater chemistry

Anhydrite plays an important if somewhat enigmatic role in the geochemical cycling of Ca, Sr, and SO_4 in MOR and back-arc hydrothermal systems (Teagle et al., 1998b; Sleep, 1991; Alt, 1995; Alt et al., 2003). The precipitation of anhydrite in and around hydrothermal recharge and discharge zones reduces porosity, permeability, and has a significant effect on the rate/geometry of hydrothermal fluid flow (Lowell et al., 2003). These physical effects engendered from anhydrite precipitation ultimately: (1)

Please cite this article in press as: Syverson D. D., et al. Experimental partitioning of Ca isotopes and Sr into anhydrite: Consequences for the cycling of Ca and Sr in subseafloor mid-ocean ridge hydrothermal systems. *Geochim. Cosmochim. Acta* (2018), https://doi.org/10.1016/j.gca.2018.03.018

insulate the oceanic crust from influx of large volumes of seawater, (2) focuses heat and flux of high-temperature fluids venting from below the seafloor; and, (3) may induce spatial variability in the extent of high temperature hydrothermal alteration of the oceanic crust (Sleep, 1991; Alt, 1995; Lowell and Yao, 2002). However, the overall mass balance of seawater sulfur predicted to be stored in young oceanic crust as anhydrite and sulfide produced from the reduction of seawater SO_4, is much less than that observed, as demonstrated by comparison of mineralogical and chemical data of drill core recovered from the relatively young oceanic drill site, DSDP/ODP Hole 504B (5.9 Ma) with thermal and geochemical estimates (Teagle et al., 1998b). This deficit, known as the anhydrite conundrum, raises the question of what particular zones in the subseafloor predominantly sequester seawater Ca and SO_4 as anhydrite, for example, along the recharge path, deep-seated at or below the lava-dike transition, or as a consequence of mixing of conductively heated seawater with hydrothermal fluid within and below the massive sulfide mound (Fig. 1). Furthermore, each anhydrite bearing zone in the subseafloor differs in the susceptibility of anhydrite dissolution upon cooling of the hydrothermal system and pervasive seawater mixing, where shallow anhydrite formed along the recharge flow path and in or below the sulfide mound is particularly sensitive to dissolution effects whereas anhydrite formed in the deep-seated zone, at or below the lava-dike transition zone, may persist on geologically significant timescales (Teagle et al., 1998b; Sleep, 1991; Alt, 1995; Alt et al., 2003). The anhydrite samples recovered and used for this study are relevant for comparison with the processes taking place particularly at the zone of seawater/hydrothermal fluid mixing in and below the massive sulfide mound (Fig. 1). In other words, the Ca and Sr isotope composition of anhydrite formed in this zone will be distinct, compositionally, relative to anhydrite formed in the recharge zones and the deep-reaction zone.

The precipitation of anhydrite, in particular in recharge zones of axial MOR hydrothermal systems, will alter the chemical and isotopic composition of fluids penetrating more deeply into the ocean crust (e.g. SW recharge zone of Fig. 1). Anhydrite precipitation will remove seawater-derived Sr, Ca, and SO_4; relatively, SO_4 will be predominantly removed if the seawater $Ca/SO_4 > 1$, whereas, the majority of Ca and Sr will be removed if seawater $Ca/SO_4 < 1$. Accordingly, the extent to which seawater Ca, SO_4, and Sr are removed from solution by anhydrite precipitation will in turn determine the extent to which these elements are available for reaction with the oceanic crust in high-temperature hydrothermal systems and chemical and isotopic fluxes associated with recycling of oceanic crust into the mantle (Bickle and Teagle, 1992; Coogan, 2008). In modern seawater, we expect all of the seawater derived Ca to be removed during anhydrite precipitation, whereas a fraction of seawater Sr is removed, upon recharge into the seafloor and effectively replaced by Ca and Sr derived from the oceanic crust. In contrast, an ancient ocean with a $Ca/SO_4 > 1$ (i.e. the Eocene), seawater derived Ca and Sr may persist beyond the zone of anhydrite precipitation near the seafloor and the partially modified isotopic signature of seawater may be incorporated into secondary Ca silicates during exchange and alteration at high temperature in the reaction zone or possibly retained in composition in the hydrothermal fluid emitting from the subseafloor (Lowenstein et al., 2001; Wortmamnn and Paytan, 2012; Coogan and Dosso, 2015; Antonelli et al., 2017). Although seawater Ca/SO_4 ratios likely play an important role in determining the $\delta^{44}Ca$ value of altered oceanic crust, these specific cause and effect processes are not well understood and require experimental and further field data to constrain the Ca isotope composition of altered and subducted oceanic crust.

4.2. Sr/Ca partitioning effects associated with anhydrite precipitation

The mass transfer of Ca and Sr between seawater, hydrothermal fluid, and the oceanic crust is sensitive to anhydrite precipitation and recrystallization in the subseafloor (Chiba et al., 1998; Petersen et al., 1998; Teagle et al., 1998a; Tivey et al., 1998; Mills and Tivey, 1999). This is demonstrated from the experimental anhydrite-fluid Sr/Ca partition data presented in this study, where the early stages of incipient anhydrite precipitation predominantly exhibit elevated K_D values between anhydrite and dissolved constituents, 1.24–0.77 (Fig. 5), relative to the long-term steady state values, 0.66–0.52. The elevated K_D values demonstrate that the distribution of Sr relative to Ca between the anhydrite-fluid reservoirs is sensitive to the initial formation conditions, in accordance with past experimental data from Shikazono and Holland (1983). Both experimental studies demonstrate that increasingly supersaturated fluids and high rates of anhydrite precipitation result in elevated K_D values, effectively approaching values of unity, similar to experimental observations made in the calcite-fluid system at wide range of temperatures (Lorens, 1981; Beck et al., 1992; Lemarchand et al., 2004; Tang et al., 2008; Lopez et al., 2009; DePaolo, 2011). Comparison of time-series K_D values from this study and K_D values from prescribed supersaturation experiments performed by Shikazono and Holland (1983) relative to equilibrium K_D values inferred from both studies, 0.20–0.40, may demonstrate reversibility throughout the range of temperatures indicative of MOR hydrothermal systems.

The observed K_D values from TAG are likely indicative of kinetic and/or reservoirs effects due to rapid anhydrite precipitation from hydrothermal solution(s), with limited exchange towards equilibrium thereafter, especially at temperatures < 350 °C (Figs. 5 and 10) (Teagle et al., 1998a; Mills and Tivey, 1999). On average, a K_D value of approximately 0.50–0.60 would represent the mean Sr/Ca partitioning value between anhydrite and hydrothermal fluid/seawater mixtures in the upper subseafloor (>50 m below the seafloor). Interestingly, K_D values from TAG vary with depth, where values exceed unity near the seafloor and have intermediate radiogenic Sr isotope compositions between MORB and seawater. However, anhydrite-fluid K_D values at >50 m below the seafloor approach values that are consistent with equilibrium conditions and have a mostly radiogenic Sr isotope signature (seawater dominated). This

Please cite this article in press as: Syverson D. D., et al. Experimental partitioning of Ca isotopes and Sr into anhydrite: Consequences for the cycling of Ca and Sr in subseafloor mid-ocean ridge hydrothermal systems. *Geochim. Cosmochim. Acta* (2018), https://doi.org/10.1016/j.gca.2018.03.018

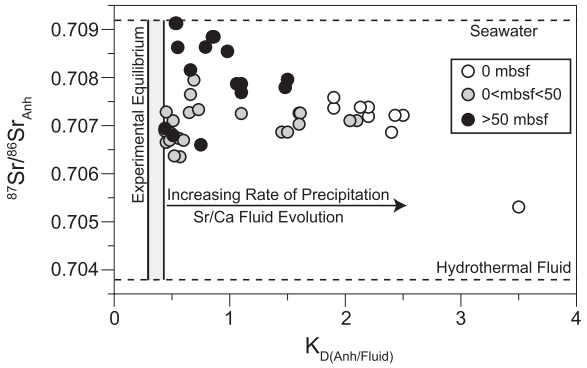

Fig. 10. Comparison of K_D values with radiogenic Sr isotope composition of anhydrite recovered from the massive sulfide mound at the TAG MOR hydrothermal system derived from the dataset produced by Mills and Tivey (1999) and Teagle et al. (1998a) relative to the equilibrium temperature dependent K_D values determined from this experimental study (grey rectangle). The open, grey, and black circles represent the depths of anhydrite sampled, 0 meters below seafloor (mbsf), 0 < mbsf < 50, and >50 mbsf, respectively. This comparison of these specific natural data relative to experimental constraints indicates that the K_D values exhibited from the TAG hydrothermal system are predominantly indicative of disequilibrium effects, likely from kinetic and reservoir effects produced upon the precipitation of anhydrite during rapid mixing of conductively heated seawater with end-member hydrothermal fluids in the subseafloor.

correlation suggests that anhydrite formed along pathways where conductively heated seawater mixed with minor amounts of end-member hydrothermal fluids, precipitates relatively slowly at near equilibrium conditions. Conversely, anhydrite that formed near the seafloor, at and below the sulfide mound, forms rapidly at far from equilibrium conditions due to dynamic mixing of end-member hydrothermal fluids and seawater (Figs. 1 and 10). These particular observations of anhydrite-fluid Sr/Ca partitioning have the potential to differentiate fluid flow pathways at hydrothermal systems.

4.3. Modern MOR Ca isotope fractionation systematics

The Ca isotope composition of the end-member TAG hydrothermal fluid, -1.19 ± 0.12‰, is lighter relative to seawater, 0‰, similar to end-member hydrothermal fluids from the Logatchev and EPR 17–19°S MOR hydrothermal systems, -0.95 ± 0.07‰ and -0.96 ± 0.19‰, respectively, and within error of MORB, -1.02 ± 0.18‰ (Schmitt et al., 2003; Amini et al., 2008; Feng et al., 2017). In comparison, the composition of the anhydrite sampled from TAG ranges from −1.03 to −1.12‰. The effect of anhydrite precipitation in the subseafloor, at and below the sulfide mound, would effectively cause the Ca isotope composition of the mixed fluids (end-member hydrothermal fluid + seawater) to become isotopically heavier (Figs. 1 and 6). Interestingly, the Ca isotope composition of seawater/hydrothermal fluid mixtures, between −0.77 and −0.46‰, determined from the coupling of the radiogenic Sr and Ca isotope composition of sampled anhydrite from the active sulfide mound of TAG and Logatchev do indicate $\delta^{44}Ca$ values greater than MORB, likely as a consequence of precipitation induced fractionation (Table 3 and Amini et al. (2008)). However, as demonstrated by TAG, Logatchev, and EPR 17–19°S end-member vent fluids, the degree of anhydrite formation in the subseafloor is not sufficient to significantly shift the Ca isotope composition of end-member fluids relative to MORB. This lack of Ca isotope compositional variability between end-member vent fluids and MORB is very likely due to the significant flux of hydrothermally derived-Ca leached from MORB, effectively overwhelming any reservoir effects caused by anhydrite precipitation in the subseafloor (Scheuermann et al., 2018). Overall, a range of −0.30 to −0.60‰ is appropriate to describe the magnitude of fractionation between anhydrite and fluid in MOR hydrothermal systems.

Primary anhydrite fluid inclusion homogenization temperature data derived from Petersen et al. (1998) from the corresponding core and similar depth interval as the sampled anhydrite used for Ca isotope analysis in this study, indicate a temperature 300–360 °C. This range of temperatures is well above that predicted from the natural anhydrite-fluid Ca isotope fractionation data reported here, approximately 150–200 °C, when compared to the tentative temperature dependent fractionation trend shown in this study (Fig. 4). This disparity is likely due to the experimental data not being indicative of equilibrium fractionation conditions upon precipitation or a reflection of the dynamic nature of fluids circulating and mixing in the subseafloor at TAG (Chiba et al., 1981, 1998; Petersen et al., 1998; Teagle et al., 1998a; Tivey et al., 1998; Shanks, 2001). Further experiments are needed to constrain the uncertainty between equilibrium and kinetic effects produced upon anhydrite precipitation to better understand the interpretation of the Ca elemental and isotopic budget of MOR hydrothermal systems.

5. CONCLUSIONS

The experimental data presented in this study address the effect of temperature and time on Sr/Ca partitioning and exchange and fractionation of Ca isotopes between fluid and anhydrite. Experimental results indicate that Sr/Ca partitioning between anhydrite and dissolved components are subject to disequilibrium effects, which change with time as anhydrite undergoes recrystallization and crystal growth. In addition, the associated Ca isotope fractionation between anhydrite and dissolved Ca^{2+} ($\Delta^{44/40}Ca_{(Anh\text{-}Fluid)}$) results in enrichment of heavy isotopes of Ca in solution, although the magnitude of this decreases with increasing temperature, consistent with previous experimental data. The addition of an enriched ^{43}Ca source to the anhydrite-bearing system allows quantification of the rate of isotopic exchange between the mineral and fluid reservoirs. Data indicate that the rate of exchange is a clear function of temperature and the apparent mechanism of anhydrite is recrystallization. Coupling of experimental ^{43}Ca exchange rate data with time-series Sr/Ca partitioning data permitted extrapolation towards complete exchange between the anhydrite-fluid reservoirs, resulting in equilibrium Sr/Ca isotope partitioning values, K_D, at 175, 250,

Please cite this article in press as: Syverson D. D., et al. Experimental partitioning of Ca isotopes and Sr into anhydrite: Consequences for the cycling of Ca and Sr in subseafloor mid-ocean ridge hydrothermal systems. *Geochim. Cosmochim. Acta* (2018), https://doi.org/10.1016/j.gca.2018.03.018

and 350 °C, of 0.43 ± 0.12, 0.34 ± 0.05, 0.29 ± 0.02 (1σ), respectively.

Physiochemical processes controlling the chemical and isotopic composition of anhydrite and hydrothermal fluid recovered from the TAG and Logatchev hydrothermal systems are informed by the experimental results. Specifically, conditions in the subseafloor where mixing of end-member hydrothermal fluid with conductively heated seawater can result in elevated K_D values owing to kinetic effects imposed by anhydrite formation from supersaturated fluids. The opposite is likely true of anhydrite precipitation along fluid pathways where temperature increase is more gradual, such as seawater recharge zones. In this case, equilibrium Sr/Ca partitioning values can be realized. Although the precipitation of anhydrite is a significant process in the subseafloor of modern MOR hydrothermal systems, the Ca isotope composition of end-member vent fluid from TAG and Logatchev remain within error of the composition of MORB. Further experimental studies and additional analyses of Ca isotope fractionation data between anhydrite, altered and secondary silicates, and dissolved Ca^{2+} from MOR hydrothermal systems are needed to properly constrain equilibrium fractionation at a range of temperatures and to better understand the mass transfer of Ca and associated elements, such as Sr, between circulating fluids in the subseafloor with the oceanic crust.

ACKNOWLEDGEMENTS

The authors would like to thank Rick Knurr for facilitating the determination of the bulk chemistry of experimental solutions/anhydrite and of the natural hydrothermal fluid/anhydrite samples. DDS would like to personally thank Elizabeth Lundstrom and Dr. Clara Blättler (Princeton University) for instruction on sample preparation and for performing the bulk of the Ca isotope analyses on the experimental and natural samples. The authors would also like to thank Dr. Benjamin Tutolo for assistance by providing the anhydrite TAG samples imperative for this study. JAH thanks the Princeton Environmental Institute (PEI) Grand Challenge Program for water-rock interactions. Funding for this study was provided by the NSF grants 1232704 and 1434798 (WES). The authors would like to thank the two anonymous reviewers, Michael Antonelli, and the guest editor, Dr. Rachel Mills, for providing constructive reviews of this manuscript. In addition, we thank the managing editor, Dr. Tom Marchitto, for facilitating the review process.

REFERENCES

Alt J. (1995) Sulfur isotopic profile through the oceanic crust: Sulfur mobility and seawater-crust sulfur exchange during hydrothermal alteration. *Geology* **23**, 585–588.

Alt J., Davidson G. J., Teagle D. A. H. and Karson J. A. (2003) Isotopic composition of gypsum in the Macquarie Island ophiolite: Implications for the sulfur cycle and the subsurface biosphere in oceanic crust. *Geology* **31**, 549–552.

Amini M., Eisenhauer A., Bohm F., Fietzke J., Bach W., Garbe-Schonberg D., Rosner M., Bock B., Lackschewitz K. S. and Hauff F. (2008) Calcium isotope (d44/40Ca) fractionation along hydrothermal pathways, Logatchev field (Mid-Atlantic Ridge, 14 450N). *Geochim. Cosmochim. Acta* **72**, 4107–4122.

Antonelli M. A., Pester N. J., Brown S. T. and DePaolo D. J. (2017) Effect of paleoseawater composition on hydrothermal exchange in midocean ridges. *Proc. Natl. Acad. Sci.*.

Archer D. (1992) Thermodynamic properties of the NaCl + H2O system II. Thermodynamic properties of NaCl(aq), NaCl2H2O (cr), and phase equilibria. *J. Phys. Chem.* **21**, 793–829.

Balcaen L., De Schrijver I., Moens L. and Vanhaecke F. (2005) Determination of the 87Sr/ 86Sr isotope ratio in USGS silicate reference materials by multi-collector ICP-mass spectrometry. *Int. J. Mass Spectrom.* **242**, 251–255.

Beck J. W., Berndt M. E. and Seyfried W. E. (1992) Application of isotopic doping techniques to evaluation of reaction kinetics and fluid/mineral distribution coefficients: An experimental study of calcite at elevated temperatures and pressures. *Chem. Geol.* **97**, 125–144.

Berndt M. E., Seyfried W. E. and Beck J. W. (1988) Hydrothermal alteration processes at mid-ocean ridge: Experimental and theoretical constraints from Ca and Sr exchange reactions and Sr isotopic ratios. *J. Geophys. Res.* **93**, 4573–4583.

Bethke C. M. (2006) *The Geochemist Workbench Release 6.0 Reaction Modeling Guide. A User Guide to React and Gtplot*. University of Illinois.

Bickle M. J. and Teagle D. A. H. (1992) Strontium alteration in the Troodos ophiolite: implications for fluid fluxes and geochemical transport in mid-ocean ridge hydrothermal systems. *Earth Planet. Sci. Lett.* **113**, 219–237.

Bischoff J. L. and Seyfried W. E. (1978) Hydrothermal chemistry of seawater from 25C to 350C. *Am. J. Sci.* **1978**, 838–860.

Blattler C. L. and Higgins J. A. (2014) Calcium isotopes in evaporites record variations in Phanerozoic seawater SO4 and Ca. *Geology* **42**, 711–714.

Blattler C. L., Miller N. R. and Higgins J. A. (2015) Mg and Ca isotope signatures of authigenic dolomite in siliceous deep-sea sediments. *Earth Planet. Sci. Lett.* **419**, 32–42.

Blundy J., Mavrogenes J., Tattitch B., Sparks S. and Gilmer A. (2015) Generation of porphyry copper deposits by gas–brine reaction in volcanic arcs. *Nat. Geosci.* **8**, 235–240.

Chiba H., Kusakabe M., Somiya S. H., Matsuo S. and Shigeyuki S. (1981) Oxygen isotope fractionation factors between anhydrite and water from 100 to 550C. *Earth Planet. Sci. Lett.* **53**, 55–62.

Chiba H., Uchiyama N. and Teagle D. A. H. (1998) Stable isotopes study of anhydrite and sulfides minerals at the TAG hydrothermal mound, mid-atlantic ridge, 26N. *Proc. Ocean Drilling Program* **158**, 85–90.

Cole D. R., Mottle M. J. and Ohmoto H. (1987) Isotopic exchange in mineral-fluid systems. II. Oxygen and hydrogen isotopic investigation of the experimental basalt-seawater system*. *Geochim. Cosmochim. Acta* **51**, 1523–1538.

Cole D. R., Ohmoto H. and Lasaga A. C. (1983) Isotopic exchange in mineral-fluid systems. I. Theoretical evaluation of oxygen isotopic exchange accompanying surface reactions and diffusion. *Geochim. Cosmochim. Acta* **47**, 1681–1693.

Coogan L. A. (2008) Reconciling temperatures of metamorphism, fluid fluxes and heat transport in the upper crust at intermediate- to fast-spreading mid-ocean ridges. *Geochem. Geophys. Geosyst.* **9**.

Coogan L. A. and Dosso S. E. (2015) Alteration of ocean crust provides a strong temperature dependent feedback on the geological carbon cycle and is a primary driver of the Sr-isotopic composition of seawater. *Earth Planet. Sci. Lett.* **415**, 38–46.

Craddock P. R., Bach W., Seewald J. S., Rouxel O., Reeves E. P. and Tivey M. A. (2010) Rare earth element abundances in hydrothermal fluids from the Manus Basin, Papua New Guinea: Indicators of sub-seafloor hydrothermal processes in back-arc basins. *Geochim. Cosmochim. Acta* **74**, 5494–5513.

Please cite this article in press as: Syverson D. D., et al. Experimental partitioning of Ca isotopes and Sr into anhydrite: Consequences for the cycling of Ca and Sr in subseafloor mid-ocean ridge hydrothermal systems. *Geochim. Cosmochim. Acta* (2018), https://doi.org/10.1016/j.gca.2018.03.018

Criss R. E. (1999) *Principles of Stable Isotope Distribution*. Oxford University Press, New York.

Criss R. E., Gregory R. T. and Taylor H. P. (1987) Kinetic theory of oxygen isotopic exchange between minerals and water. *Geochim. Cosmochim. Acta* **51**, 1099–1108.

DePaolo D. J. (2011) Surface kinetic model for isotopic and trace element fractionation during precipitation of calcite from aqueous solutions. *Geochim. Cosmochim. Acta* **75**, 1039–1056.

Dubinina E. O. and Lakshtanov L. Z. (1997) A kinetic model of isotopic exchange in dissolution-precipitation processes. *Geochim. Cosmochim. Acta* **61**, 2265–2273.

Edmond J. M., Campbell A. C., Palmer M. R., Klinkhammer G. P., German C. R., Edmonds H. N., Elderfield H., Thompson G. and Rona P. A. (1995) Time series studies of vent fluid from the TAG and MARK sites (1986, 1990) Mid-Atlantic Ridge: a new solution chemistry model and a mechanism for Cu/Zn zonation in massive sulphide orebodies. In *Hydrothermal Vents and Processes* (eds. L. M. Parson, C. L. Walker and D. R. Dixon), pp. 77–86.

Fantle M. S. and Higgins J. (2014) The effects of diagenesis and dolomitization on Ca and Mg isotopes in marine platform carbonates: Implications for the geochemical cycles of Ca and Mg. *Geochim. Cosmochim. Acta* **142**, 458–481.

Fantle M. S. and Tipper E. T. (2014) Calcium isotopes in the global biogeochemical Ca cycle: Implications for development of a Ca isotope proxy. *Earth Sci. Rev.* **129**, 148–177.

Faure G. and Mensing T. M. (2005) *Isotopes: Principles and Applications*. John Wiley & Sons Inc, Hoboken, N.J..

Feng L. P., Zhou L., Yang L., DePaolo D. J., Tong S. Y., Liu Y. S., Owens T. L. and Gao S. (2017) Calcium isotopic compositions of sixteen USGS reference materials. *Geostandards Geoanal. Res.* **41**, 93–106.

Gothmann A. M., Bender M. L., Blattler C. L., Swart P. K., Giri S. J., Adkins J. F., Stolarski J. and Higgins J. A. (2016) Calcium isotopes in scleractinian fossil corals since the Mesozoic: Implications for vital effects and biomineralization through time. *Earth Planet. Sci. Lett.* **444**, 205–214.

Gregory R. T., Criss R. E. and Taylor H. P. (1989) Oxygen isotope exchange kinetics of mineral pairs in closed and open systems: applications to problems of hydrothermal alteration of igneous rocks and precambrian iron formations. *Chem. Geol.* **75**, 1–42.

Handler R. M., Frierdich A. J., Johnson C. M., Rosso K. M., Beard B. L., Wang C., Latta D. E., Neumann A., Pasakarnis T., Premaratne W. A. P. J. and Scherer M. M. (2014) Fe(II)-catalyzed recrystallization of goethite revisted. *Environ. Sci. Technol.* **48**, 11302–11311.

Helgeson H. C., Kirkham D. H. and Flowers G. C. (1981) Theoretical prediction of the thermodynamic behavior of aqueous electrolytes at high pressures and temperatures: IV. Calculation of activity coefficients, osmotic coefficients, and apparent molal and standard and relative partial molal properties to 600C and 5 KB. *Am. J. Sci.* **281**, 1249–1516.

Hensley T. M. and MacDougall J. D. (2003) Calcium isotope fractionation in Ca-bearing phases of marine evaporites. *Eos Trans. AGU* **46**, 84.

Herzig, P.M., Humphris, S.E., Miller, D.J., Zierenberg, R.A., 1998. Proc. ODP, Sci. Results, 158. Ocean Drilling Program, College Station, Texas.

Humphris S. E. (1998) Rare earth element composition of anhydrite: implications for depositions and mobility within the active TAG hydrothermal mound. *Proc. Ocean Drilling Program* **158**, 143–159.

Humphris S. E. and Bach W. (2005) On the Sr isotopes and REE compositions of anhydrites from the TAG seafloor hydrothermal system. *Geochim. Cosmochim. Acta* **69**, 1511–1525.

Humphris S. E., Herzig P. M., Miller D. J., Alt J., Becker K., Brown D. G. B., Chiba H., Fouquet Y., Gemmell J. B., Guerin G., Hannington M. D., Holm N. G., Honnorez J. J., Iturrino G. J., Knott R., Ludwig R., Nakamura K. S. P., Reysenbach A. L., Rona P. A., Smith S., Sturz A. A., Tivey M. K. and Zhao X. (1995) The interal structure of an active sea-floor mass sulphide deposit. *Nature* **377**, 713–716.

Humphris S. E., Tivey M. K. and Tivey M. A. (2015) The Trans-Atlantic Geotraverse hydrothermal field: A hydrothermal system on an active detachment fault. *Deep-Sea Res. II* **121**, 8–16.

Husson J. M., Higgins J. A., Maloof A. C. and Schoene B. (2015) Ca and Mg isotope constraints on the origin of Earth's deepest delta C-13 excursion. *Geochim. Cosmochim. Acta* **160**, 243–266.

Johnson C. M., Beard B. L. and Albarede F. (2004) Overview and general concepts. *Non-traditional Isotopes*, 1–24.

Johnson C. M., Skulan J. L., Beard B. L., Sun H., Nealson K. H. and Braterman P. S. (2002) Isotopic fractionation between Fe (III) and Fe(II) in aqueous solutions. *Earth Planet. Sci. Lett.* **195**, 141–153.

Kong X.-Z., Tutolo B. M. and Saar M. O. (2013) DBCreate: A SUPCRT92-based program for producing EQ3/6, TOUGHREACT, and GWB thermodynamic databases at user-defined T and P. *Comput. Geosci.* **51**, 415–417.

Lemarchand D., Wasserburg G. J. and Papanastassiou D. A. (2004) Rate-controlled calcium isotope fractionation in synthetic calcite. *Geochim. Cosmochim. Acta* **68**, 4665–4678.

Lopez O., Zuddas P. and Faivre D. (2009) The influence of temperature and seawater composition on calcite crystal growth mechanisms and kinetics: implications for Mg incorporation in calcite lattice. *Geochim. Cosmochim. Acta* **73**, 337–347.

Lorens R. B. (1981) Sr, Cd, Mn and Co distribution coefficients in calcite as a function of calcite precipitation rate. *Geochim. Cosmochim. Acta* **45**, 553–561.

Lowell R. P. and Yao Y. (2002) Anhydrite precipitation and the extent of hydrothermal recharge zones at ocean ridge crests. *J. Geophys. Res.* **107**, EPM 2-1-EPM 2-9.

Lowell R. P., Yao Y. and Germanovich L. (2003) Anhydrite precipitation and the relationship between focused and diffuse flow in seafloor hydrothermal systems. *J. Geophys. Res.* **108**.

Lowenstein T. K., Timofeef M. N., Brennan S. T., Hardie L. A. and Demicco R. V. (2001) Oscillations in phanerozoic seawater chemistry: evidence from fluid inclusions. *Science* **294**, 1086–1088.

McDermott J. M., Ono S., Tivey M. K., Seewald J. S., Shanks W. C. and Solow A. R. (2015) Identification of sulfur sources and isotopic equilibria in submarine hot-springs using multiple sulfur isotopes. *Geochim. Cosmochim. Acta* **160**, 169–187.

Mills R. A., Teagle D. A. H. and Tivey M. A. (1998) Fluid mixing and anhydrite precipitation within the TAG mound. *Proc. Ocean Drilling Program* **158**, 119–127.

Mills R. A. and Tivey M. K. (1999) Seawater entrainment and fluid evolution within the TAG hydrothermal mound: evidence from analyses of anhydrite. *Mid-ocean Ridges: Dynamics of Processes Associated with Creation of New Ocean Crust*, 225–263.

Nadeau O. (2015) Economic geology: Ore metals beneath volcanoes. *Nat. Geosci.* **8**, 168–170.

Newton R. C. and Manning C. E. (2004) Solubility of anhydrite, CaSO4, in NaCl-H2O solutions at high pressures and temperatures: applications to fluid-rock interaction. *J. Petrol.* **46**, 701–716.

Ohmoto H. and Lasaga A. C. (1982) Kinetics of reactions between aqueous sulfates and sulfides in hydrothermal systems. *Geochim. Cosmochim. Acta* **46**, 18.

Please cite this article in press as: Syverson D. D., et al. Experimental partitioning of Ca isotopes and Sr into anhydrite: Consequences for the cycling of Ca and Sr in subseafloor mid-ocean ridge hydrothermal systems. *Geochim. Cosmochim. Acta* (2018), https://doi.org/10.1016/j.gca.2018.03.018

Ohmoto H. and Rye R. O. (1979) Isotopes of sulfur and carbon. In *Geochemistry of Hydrothermal Ore Deposits* (ed. H. L. Barnes). J Wiley and Sons, pp. 509–567.

Ono S., Shanks W. C., Rouxel O. J. and Rumble D. (2007) S-33 constraints on the seawater sulfate contribution in modern seafloor hydrothermal vent sulfides. *Geochim. Cosmochim. Acta* **71**, 1170–1182.

Peters M., Strauss H., Farquhar J., Ockert C., Eickmann B. and Jost C. L. (2010) Sulfur cycling at the mid-atlantic ridge: a multiple sulfur isotope approach. *Chem. Geol.* **269**, 180–196.

Petersen S., Herzig P. M. and Hannington M. D. (1998) Fluid inclusion studies as a guide to temperature regime within the TAG hydrothermal mound. *Proc. Ocean Drilling Program* **158**, 163–176.

Rona P. A., Klinkhammer G., Nelsen T. A., Trefry J. H. and Elderfield H. (1986) Black smokers, massive sulfides, and vent biota on the Mid-Atlantic Ridge. *Nature* **321**, 33–37.

Scheuermann P. P., Syverson D. D., Higgins J. A., Pester N. J. and Seyfried W. E. (2018) Calcium isotope systematics at hydrothermal conditions: Mid-ocean ridge vent fluids and experiments in the CaSO4-NaCl-H2O system. *Geochim. Cosmochim. Acta* **226**, 18–35.

Schmitt A. D., Chabaux F. and Stille P. (2003) The calcium riverine and hydrothermal isotopic fluxes and the oceanic calcium mass balance. *Earth Planet. Sci. Lett.* **213**, 503–518.

Seewald J. S., Doherty K. W., Hammar T. R. and Liberatore S. P. (2001) A new gas-tight isobaric sampler for hydrothermal fluids. *Deep-Sea Res. I* **49**, 189–196.

Seyfried W. E. and Ding K. (1993) The effect of redox on the relative solubilities of copper and iron in Cl-bearing aqueous fluids at elevated temperatures and pressures: An experimental study with application to subseafloor hydrothermal systems. *Geochim. Cosmochim. Acta* **57**, 1905–1917.

Seyfried W. E., Janecky D. R. and Berndt M. E. (1987) Rocking autoclaves for hydrothermal experiments: II. The flexible reaction-cell system. *Hydrothermal Exp. Tech.*, 216–239.

Shanks W. C. (2001). *Rev. Mineral. Geochem.* **43**, 469–525.

Shikazono H. and Holland H. D. (1983) The partitioning of strontium between anhydrite and aqueous solution from 150 to 250C. *Econ. Geol. Monogr.* **5**, 320–328.

Shock E. L., Helgeson H. C. and Sverjensky D. A. (1989) Calculation of the thermodynamic and transport properties of aqueous species at high pressures and temperatures: Standard partial molal properties of inorganic neutral species. *Geochim. Cosmochim. Acta* **53**, 2157–2183.

Shock E. L., Oelkers E. H., Johnson J. W., Sverjensky D. A. and Helgeson H. C. (1992) Calculatiion of the thermodynamic properties of aqueous species at high pressures and temperatures: effective electrostatic radii, dissociation constants, and standard partial molal properties to 1000C and 5 kbar. *J. Chem. Soc., Faraday Transactions* **88**, 803–826.

Shock E. L., Sassani D. C., Willis M. and Sverjensky D. A. (1997) Inorganic species in geologic fluids: correlations among standard molal thermodynamic properties of aqueous ions and hydroxide complexes. *Geochim. Cosmochim. Acta* **61**, 907–950.

Sleep N. H. (1991) Hydrothermal circulation, anhydrite precipitation, and thermal structure at ridge axes. *J. Geophys. Res.* **96**, 2375–2387.

Sverjensky D. A., Shock E. L. and Helgeson H. C. (1997) Prediction of the thermodynamic properties of aqueous metal complexes to 1000C and 5 kbar. *Geochim. Cosmochim. Acta* **61**, 1359–1412.

Tang J., Dietzel M., Bohm F., Kohler S. J. and Eisenhauer A. (2008) Sr2+/Ca2+ and 44Ca/40Ca fractionation during inorganic calcite formation: II. Ca isotopes. *Geochim. Cosmochim. Acta* **72**, 3733–3745.

Tanger J. C. and Helgeson H. C. (1988) Calculation of the thermodynamic and transport properties of aqueous species at high pressures and temperatures: revised equations of state for the standard partial molal properties of ions and electrolytes. *Am. J. Sci.* **288**.

Teagle D. A. H., Alt J., Chiba H. and Halliday A. N. (1998a) Dissecting an active hydrothermal deposit: The strontium and oxygen isotopic anatomy of the TAG hydrothermal mound-anhydrite. *Proc. Ocean Drilling Program* **158**, 129–141.

Teagle D. A. H., Alt J. and Halliday A. N. (1998b) Tracing the chemical evolution of fluids during hydrothermal recharge: Constraints from anhydrite recovered in ODP Hole 504B. *Earth Planet. Sci. Lett.* **155**, 167–182.

Tivey M. K., Humphris S. E., Thompson G., Hannington M. D. and Rona P. A. (1995) Deducing patterns of fluid flow and mixing within the active TAG mound using mineralogical and geochemical data. *J. Geophys. Res.* **100**, 12,527-512,555.

Tivey M. K., Mills R. A. and Teagle D. A. H. (1998) Temperature and salinity of fluid inclusions in anhydrite as indicators of seawater entrainment and heating in the TAG active mound. *Proc. Ocean Drilling Program* **158**, 179–190.

Tolstoy M., Waldhauser F., Bohnenstiehl D. R., Weekly R. T. and Kim W. Y. (2008) Seismic identification of along-axis hydrothermal flow on the East Pacific Rise. *Nature* **451**, 181–184.

Wortmamnn U. G. and Paytan A. (2012) Rapid variability of seawater chemistry over the past 130 millions years. *Science* **337**, 334–336.

Wu S.-J., Yang C.-J., Pester N. J. and Chen Y. (2011) A new hydraulically actuated titatium sampling valve for deep-sea hydrothermal fluid samples. *IEEE J. Oceanic Eng.* **36**, 462–469.

You C.-F. and Bickle M. J. (1998) Evolution of an active sea-floor massive sulphide deposit. *Nature* **394**, 668–671.

Associate editor: Thomas M. Marchitto

Please cite this article in press as: Syverson D. D., et al. Experimental partitioning of Ca isotopes and Sr into anhydrite: Consequences for the cycling of Ca and Sr in subseafloor mid-ocean ridge hydrothermal systems. *Geochim. Cosmochim. Acta* (2018), https://doi.org/10.1016/j.gca.2018.03.018